MANUSCRIPT

Prediction and quantification of hepatic transporter-mediated uptake of pitavastatin utilizing a combination of the Relative Activity Factor approach and mechanistic modeling

Pallabi Mitra, Samantha Weinheimer, Meeghan Michalewicz, and Mitchell E. Taub

Drug Metabolism and Pharmacokinetics Department, Boehringer Ingelheim Pharmaceuticals, Inc., Ridgefield, CT 06877

Running title: Quantification of hepatic uptake of pitavastatin

Corresponding author: Pallabi Mitra

Drug Metabolism and Pharmacokinetics Department,

Boehringer Ingelheim Pharmaceuticals, Inc.

900 Ridgebury Road, Ridgefield, CT 06877

Tel: 203-798-5766

Fax: 203-791-6003

Email: pallabi.mitra@boehringer-ingelheim.com

Number of text pages: 47

Number of tables: 5

Number of figures: 3

Number of references: 47

No. of supplemental tables: 3

No. of supplemental figures: 5

Abstract word count: 242

Introduction word count: 742

Discussion word count: 1492

Nonstandard abbreviations:

AUC, area under the plasma concentration-time curve; AUCR, ratio of AUCs obtained in the presence and absence of an inhibitor; CCK8, cholecystokinin octapeptide; $CL_{passive}$, passive diffusional clearance; $CL_{transporter}$, uptake clearance by a particular transporter; DDI, drug-drug interactions; DRF, dynamic RAF approach; E3S, Estrone-3-sulfate; f_t, fraction transported by a

particular transporter; f_h, fraction escaping hepatic metabolism; $f_{u,cell}$, fraction unbound in cells; $f_{u,med}$, fraction unbound in medium IVIVC, in vitro in vivo correlations; KHB, Krebs-Henseleit buffer; K_i, reversible inhibition constant ; NCE, new chemical entity; PBPK, physiologically based PK modeling; RAF, relative activity factor; REF, relative expression factor; SCHH, sandwich cultured human hepatocytes; SDS, sodium dodecyl sulfate; TCA, taurocholic acid

DMD Fast Forward. Published on April 17, 2018 as DOI: 10.1124/dmd.118.080614
This article has not been copyedited and formatted. The final version may differ from this version.

Abstract

Quantification of the fraction transported (f_t) by a particular transporter will facilitate more robust estimations of transporter interactions. Using pitavastatin as a model uptake transporter substrate, we investigated the utility of the relative activity factor (RAF) approach and mechanistic modeling, to estimate f_t in hepatocytes. Transporters evaluated were OATP1B1, OATP1B3, and NTCP. Transporter expressing HEK293 cells and human hepatocytes were used for determining RAF values, which were then incorporated into the mechanistic model to simulate hepatocyte uptake of pitavastatin over time. There was excellent agreement between simulated and observed hepatocyte uptake of pitavastatin indicating the suitability of this approach for translation of uptake from individual transporter-expressing cells to more holistic in vitro models. Subsequently, f_t values were determined. The largest contributor to hepatocyte uptake of pitavastatin was found to be OATP1B1, which correlates with what is known about the in vivo disposition of pitavastatin. The f_t values were then used for evaluating in vitro in vivo correlations (IVIVC) of hepatic uptake inhibition with OATP inhibitors rifampicin and cyclosporine. Predictions were compared with previously-reported plasma exposure changes of pitavastatin with these inhibitors. Although hepatic uptake inhibition of pitavastatin was 2-3X under predicted, incorporation of scaling factors (SFs) into RAF values significantly improved the predictive ability. We propose that calibration of hepatocytes with standard transporter substrates and inhibitors would allow for determination of system-specific SFs, which subsequently could be used for refining predictions of clinical DDI potential for NCEs that undergo active hepatic uptake.

.

DMD Fast Forward. Published on April 17, 2018 as DOI: 10.1124/dmd.118.080614
This article has not been copyedited and formatted. The final version may differ from this version.

Introduction

For a new chemical entity (NCE), in vitro evaluation as a potential substrate and inhibitor of key drug transporters aids in estimating the likelihood of drug-drug interactions (DDIs). If the NCE is a substrate of one or more of these key transporters in vitro, then a clinical trial involving concomitant administration with a selective inhibitor may be required. Results of such a study can then be extrapolated to estimate the DDI potential for other concomitantly administered drugs that interact with the same clearance pathway. However, this can be a resource demanding path forward for a compound in clinical development, and may not be the most efficient way to ensure patient safety. As such, a bridge between these two steps, i.e. establishing a more mechanistically-derived in vitro in vivo correlation (IVIVC) could in principle provide improved estimation of the extent to which the disposition of the NCE would be affected by inhibition of a particular transporter. Such analyses can then guide clinical teams more confidently regarding the need for a clinical DDI study.

IVIVCs for substrate-level interactions with transporters require quantification of the fraction of the substrate transported by a particular transporter (f_t). To approximate f_t values with human transporters, several in vitro techniques can be explored. The most commonly used approach for estimating f_t is inhibition of uptake (Shitara et al., 2003; Bi et al., 2012; Bi et al., 2013; Ramsden et al., 2014). Although less common, use of siRNA is another technique (Williamson et al., 2013). Modeling in vitro hepatocyte uptake is a third method that can be used to estimate various clearance pathways (uptake, metabolism, biliary excretion); however, this method usually does not facilitate dissection of individual transporter contributions (Jones et al., 2012; Menochet et al., 2012b; Menochet et al., 2012a). The relative activity factor (RAF) and relative expression factor (REF) approaches, which involve translation of transporter interactions from individual

transporter-expressing cells to more holistic models such as hepatocytes, can also be used for estimating f_t and have the benefit of using specific uptake in expression systems to better understand the integrated uptake in hepatocytes (Hirano et al., 2004; Kimoto et al., 2012; Kunze et al., 2014).

Most published studies employing RAF/REF techniques have employed static approaches of f_t estimation, whereby RAF/REF values for each uptake transporter were determined and subsequently used for estimating hepatocyte uptake clearance via each transporter (CL_i). The f_t value was estimated by expressing CL_i as a fraction of total predicted hepatocyte uptake clearance. While useful, this static approach lacked the integration of multiple processes occurring simultaneously over time. Recently however, the scope of the REF approach was expanded to integrate other processes (passive diffusion and efflux transport) and for predicting hepatocyte uptake over time as a function of all of these processes (Vildhede et al., 2016). This more dynamic method provided substantial improvement in identification of transporters that were most critical to hepatocyte uptake and elimination of pitavastatin. A dynamic approach was also recently employed to estimate RAF and renal clearance from data obtained in individually transfected HEK293 cells; however, the lack of a holistic in vitro model for the kidney limits the translation of data from individually transfected HEK293 cells to such a holistic model (Mathialagan et al., 2017). To date, the RAF approach has not been employed for dynamic predictions of cellular uptake of a compound that is a substrate of multiple hepatic uptake transporters, nor has it been utilized for estimating f_t, via extrapolation from transfected cells to hepatocytes. The primary advantage of such a dynamic approach is the ability to integrate multiple processes (passive diffusion, uptake, efflux, and metabolism), and thus, in principle, providing a more integrated value for f_t when compared to static methods.

In this study, a similar dynamic approach, as used by Vildehede et.al, has been used to estimate f_t of hepatocyte uptake of pitavastatin (Vildhede et al., 2016). However, RAF, not REF, was used as the quantitation method. In this approach, henceforth referred to as the "dynamic RAF approach (DRF)", uptake of pitavastatin into hepatocytes was predicted by integrating multiple uptake transporter clearances, bidirectional passive diffusion, and basolateral efflux clearance. Pitavastatin was chosen as the test compound, since the predominant hepatic elimination pathway of pitavastatin is active uptake (Watanabe et al., 2010; Jigorel and Houston, 2012; Riede et al., 2016). Following prediction of hepatocyte uptake, f_t values were estimated and subsequently employed for estimating IVIVC of hepatic uptake inhibition, as a means of predicting clinical outcomes.

DMD Fast Forward. Published on April 17, 2018 as DOI: 10.1124/dmd.118.080614
This article has not been copyedited and formatted. The final version may differ from this version.

Materials and Methods

Chemicals and Reagents

[^{3}H]-Estrone-3-sulfate (E3S, 50 Ci/mmol), [^{3}H]-pitavastatin (5 Ci/mmol) were purchased from American Radiolabeled Chemicals (St. Louis, MO). [^{3}H] Cholecystokinin octapeptide (CCK-8, 98.7 Ci/mmol) and [^{3}H]-taurocholic acid (TCA, 10 Ci/mmol) were bought from Perkin Elmer (Shelton, CT). Pitavastatin calcium was purchased from Santa Cruz (Dallas, TX), CCK-8 was obtained from Phoenix Pharmaceuticals, Inc. (Burlingame, CA), while estrone-3-sulfate sodium salt, and taurocholic acid sodium salt were bought from Sigma-Aldrich (Burlington, MA). Cryopreserved human hepatocytes lots HUM4122D and HUP1001 were purchased from Lonza (Walkersville, IL) while lots Hu1651 and Hu8110 were bought from Life Technologies (Carlsbad, CA). Donor characteristics are provided in the supplementary section (Table S1).

In vitro transport studies

OATP and NTCP substrate assays in human embryonic kidney (HEK293) cells:

HEK293 cells were maintained and transiently transfected with human OATP1B1, OATP1B3, NTCP, or vector-control cDNA as per previously-published procedures (Taub et al., 2011). All uptake assays were conducted at 37 ^{o}C. Total uptake was determined from uptake in transporter-transfected cells, while passive uptake was determined from uptake in vector-transfected cells. The linear range of time-dependent uptake was assessed from initial experiments (data not shown). Subsequently, the incubation time of each substrate selected for concentration-dependent uptake assays was as follows: 1 minute for E3S and pitavastatin, and 3 min for TCA and CCK-8. Uptake assays were initiated by adding either radiolabeled compound or a mixture

DMD Fast Forward. Published on April 17, 2018 as DOI: 10.1124/dmd.118.080614
This article has not been copyedited and formatted. The final version may differ from this version.

of radiolabeled compound and non-radiolabeled compound to each well. Assays were conducted and samples were lysed as published previously (Taub et al., 2011). Cellular uptake was quantified by liquid scintillation counting. The total cellular protein content was determined by the Bradford method (Stoscheck, 1990).

Hepatocyte selection: Donor characteristics and uptake characteristics of hepatocyte lots are provided in the supplementary section (Table S1). Hepatocyte lots were selected based upon vendor-certification of uptake activity and further qualified in-house with respect to active uptake of E3S. Hepatocyte lots that exhibited significant active uptake of E3S were used for this study.

OATP and NTCP substrate assays in hepatocytes in suspensions: The oil-spin centrifugation method was used to assess uptake in hepatocyte suspensions and was based on protocol of Bioreclamation IVT. As this protocol can no longer be accessed on the supplier's website, details of the assay have been provided in Section 2 of the supplemental text. For all compounds, total uptake was evaluated at 37^{o}C, and passive uptake was evaluated at 4 ^{o}C. Additionally for E3S, passive uptake was also evaluated at 37^{o}C in the presence of 100 µM rifamycin SV, an inhibitor of OATP1B1 and OATP1B3. Initial experiments were conducted to determine the linear range of time-dependent uptake. Subsequently, the incubation times selected for concentration-dependent uptake assays were as follows: 1 minute for E3S and pitavastatin, and 3 minutes for TCA and CCK-8. Substrate solutions were prepared in Krebs-Henseleit buffer (KHB) for all assays except when assessing passive diffusion by NTCP where sodium-free buffer was prepared as described previously (Taub et al., 2011) . Uptake assays were conducted with either only radiolabeled compound or a mixture of radiolabeled compound and non-radiolabeled compound. The only change made to the supplier's protocol was that following

DMD Fast Forward. Published on April 17, 2018 as DOI: 10.1124/dmd.118.080614
This article has not been copyedited and formatted. The final version may differ from this version.

centrifugation through the oil layer, each tube was placed on dry ice for at least 20 min. The tubes were then cut, and the bottom layer of each tube containing the cell pellet was lysed in 1% sodium dodecyl sulfate (SDS) solution. Samples were quantified by liquid scintillation counting, and total cellular protein content was determined by the Bradford method (Stoscheck, 1990).

OATP and NTCP substrate assays in sandwich cultured human hepatocytes (SCHH): Single donor primary human hepatocytes were cultured according to the protocols of the supplier (Lonza Suspension and Plateable Cryopreserved Hepatocytes protocol). Further details of the assay have been provided in Section 2 of the supplemental text. At approximately 24 h after plating, cells were overlaid with Matrigel. Uptake assays were conducted 5 days after the addition of Matrigel to allow formation of bile canaliculi (Vildhede et al., 2016). For all compounds, total uptake was assessed at 37^{o}C while passive uptake was evaluated at 4^{o}C. Passive uptake of E3S was also evaluated at 37^{o}C in the presence of 100 uM rifamycin SV. Initial experiments were conducted to determine linearity of time-dependent uptake. Subsequently, the incubation times selected for concentration-dependent uptake assays were as follows: 1 minute for E3S and pitavastatin, and 3 minutes for TCA and CCK-8. The uptake buffer was KHB for all assays except when assessing passive diffusion by NTCP where sodium-free buffer was prepared as described previously (Taub et al., 2011). For initiation of uptake studies, substrate solutions containing either radiolabeled compound or a mixture of radiolabeled compound and non-radiolabeled compound was added to each well. At the end of the incubation, the incubation buffer was collected. The cells were washed with ice cold buffer, and lysed in 1% SDS. The incubation buffers (before and after incubation) and the cellular lysates were quantified by liquid scintillation counting to determine amounts of compound in the incubation medium and cells respectively. Total cellular protein content was determined by the Bradford

method. Protein concentrations of control wells containing Matrigel only, were subtracted from total protein concentrations determined from wells containing cells and Matrigel, in order to determine the amount of protein associated with cells.

Determination of kinetic constants of active uptake and RAF values

In all transport assays above, active uptake was determined by subtracting passive uptake from total uptake. The active uptake of each substrate was subsequently subjected to Eadie-Hofstee transformations. In situations where biphasic uptake profiles were observed in the Eadie-Hofstee plots, only the high affinity component of uptake (saturable component) was considered for estimating kinetic constants (K_m and V_{max}) using the Michaelis-Menten equation as shown below in equation 1. GraphPad Prism (v6) was used for the analyses.

$$V = \frac{V_{max}.[S]}{K_m + [S]} \quad \text{.....(1)}$$

where, V is the active uptake rate (pmol/min/mg protein), V_{max} is the predicted maximal active uptake rate, [S] is the substrate concentration (µM), and K_m is the substrate concentration at which V_{max} is half of the maximum value.

Uptake clearances (CL_{int}, µL/min/mg protein) for each substrate were subsequently estimated as shown in equation 2.

$$CL_{int} = \frac{V_{max}}{K_m} \quad \text{.....(2)}$$

The RAF is defined as the ratio of clearance in human hepatocytes to clearance in transfected cells (Chapy et al., 2015), and was calculated from equation 3.

$$\text{RAF} = \frac{\text{CL}_{\text{int,hepatocytes}}}{\text{CL}_{\text{int,HEK}}} \quad \ldots\ldots\ldots\ldots\ldots\ldots\ldots(3)$$

RAF values for OATP1B1, OATP1B3, and NTCP were calculated from uptake kinetics of E3S, CCK-8, and TCA, respectively. It is well known that CCK-8 and TCA are selective substrates of OATP1B3 and NTCP, and this was found to be true in initial experiments. E3S has previously been used as a selective OATP1B1 substrate for RAF purposes (Hirano et al., 2004; Kunze et al., 2014). E3S is a substrate of NTCP as well and small portion of the uptake of E3S in hepatocytes is facilitated by NTCP, this was further corrected as follows: the uptake clearance of E3S in HEK-NTCP was multiplied by the hepatocyte RAF-NTCP values to obtain an estimate of the NTCP-mediated clearance of E3S in hepatocytes. The estimated NTCP-mediated E3S clearance in hepatocytes was subsequently subtracted from the observed E3S active uptake clearance in hepatocytes. The resulting E3S uptake clearance in hepatocytes was considered to be reflective of OATP1B1-mediated uptake clearance in hepatocytes and was used for determining RAF of OATP1B1.

Mechanistic model of in vitro hepatocyte disposition of pitavastatin

A two compartment model was constructed in Phoenix WinNonlin (v 6.3) to represent the hepatocyte uptake process (equations 4 and 5), with the two compartments representing the media and the cells.

$$\frac{\text{dA}_{\text{med}}}{\text{dt}} = -\left(\text{CL}_{\text{passive}} + \text{CL}_{\text{OATP1B1}} + \text{CL}_{\text{OATP1B3}} + \text{CL}_{\text{NTCP}}\right) * (\text{C}_{\text{med}} * \text{f}_{\text{u,med}}) - (\text{NSB} * (\text{C}_{\text{med}} * \text{f}_{\text{u,med}}) + \left(\text{CL}_{\text{passive}} + \text{CL}_{\text{MRP3}} + \text{CL}_{\text{BCRP}} + \text{CL}_{\text{Pgp}}\right) * (\text{C}_{\text{cell}} * \text{f}_{\text{u,cell}}) \quad \ldots\ldots..(4)$$

DMD Fast Forward. Published on April 17, 2018 as DOI: 10.1124/dmd.118.080614
This article has not been copyedited and formatted. The final version may differ from this version.

$$\frac{dA_{cell}}{dt} = +\left(CL_{passive} + CL_{OATP1B1} + CL_{OATP1B3} + CL_{NTCP}\right) * (C_{med} * f_{u,med}) -$$

$$\left(CL_{passive} + CL_{MRP3} + CL_{BCRP} + CL_{Pgp}\right) * (C_{cell} * f_{u,cell}) \quad \text{.....(5)}$$

Where, $A_{med\ or\ cell}$ is the amount of substrate in medium or cell at time t; and $C_{med\ or\ cell}$ is the total concentration of compound in the medium or cells at time t. $V_{med\ or\ cell}$ (volume of media or cells) was used to estimate $C_{med\ or\ cell}$, and V_{med} was 500 µL and 150 µL for hepatocytes in sandwich-culture and suspension respectively. V_{cell} was considered to be 3.9 µL/million cells for hepatocytes in suspension (Menochet et al., 2012b) and 7.4 µL/mg total protein for SCHH (Pfeifer et al., 2013). $f_{u,med}$ is the fraction unbound in media (=1) and $f_{u,cell}$ is the fraction unbound in cells. NSB (non-specific binding) is the fraction of pitavastatin lost per min due to nonspecific binding between the first and last sampling time points (units are min^{-1}).

CL refers to clearance mediated by either passive diffusion ($CL_{passive}$) or transporters. Equations 4 and 5 show all transporters that are known to affect the hepatocyte disposition of pitavastatin. However, in suspension hepatocytes, biliary networks are not known to form. In SCHH, in this case, the experimental setup did not differentiate between accumulation between cells and between bile. Hence, in both situations, CL_{BCRP} and $CL_{P\text{-}gp}$ were considered to be 0. Thus, hepatocyte disposition of pitavastatin was modeled through equations 6 and 7 as shown below. Of note, the error codes associated with both C_{med} and C_{cell} were additive.

$$\frac{dA_{med}}{dt} = -\left(CL_{passive} + CL_{OATP1B1} + CL_{OATP1B3} + CL_{NTCP}\right) * (C_{med} * f_{u,med}) - (NSB *$$

$$(C_{med} * f_{u,med}) + \left(CL_{passive} + CL_{MRP3}\right) * (C_{cell} * f_{u,cell}) \quad \text{.....(6)}$$

DMD Fast Forward. Published on April 17, 2018 as DOI: 10.1124/dmd.118.080614
This article has not been copyedited and formatted. The final version may differ from this version.

$$\frac{dA_{cell}}{dt} = +\left(CL_{passive} + CL_{OATP1B1} + CL_{OATP1B3} + CL_{NTCP}\right) * (C_{med} * f_{u,med}) -$$

$$\left(CL_{passive} + CL_{MRP3}\right) * (C_{cell} * f_{u,cell}) \quad \ldots\ldots\ldots(7)$$

Transporter-mediated uptake clearance ($CL_{transporter}$) in equations (6) and (7) above were further delineated as shown in Equation 8:

$$CL_{uptake\ transporter} = \frac{V_{max}.RAF}{K_m + [C_{med} * f_{u,med}]} \quad \ldots\ldots\ldots\ldots(8)$$

Where, V_{max} and K_m are the uptake kinetic constants of pitavastatin determined in the HEK293 cells for a particular transporter, and RAF is the corresponding RAF of the transporter. The only efflux transporter pertinent to our experimental set-up was MRP3. For MRP3, the efflux clearance parameters were obtained from the literature (Vildhede et al., 2016) and were not estimated in this experiment.

Due to non-specific binding of pitavastatin (experimentally estimated to be 10-20%), the initial amount available to the cells was determined from either buffer incubations on plastic at 1 min (the shortest time point), or from total radioactivity recovered in buffer and cells at 1 min, whichever value was highest. Of note, it has been reported that $f_{u,med}$ of pitavastatin (obtained from fitting) can be as low as 0.63 (Menochet et al., 2012b), which presumably is due to non-specific binding of pitavastatin.

Determination of fraction unbound in cell ($f_{u,cell}$) and $CL_{passive}$

$CL_{passive}$ and $f_{u,cell}$ were derived by fitting hepatocyte disposition of pitavastatin at 4°C to the two-compartment model (equations 4 and 5 above). All transporter-associated clearances were fixed to 0 (under the assumption that active processes are not functional at 4°C). Loss of pitavastatin

from media and uptake of pitavastatin into cells were simultaneously fit to obtain $CL_{passive}$ and $f_{u,cell}$.

The $f_{u,cell}$, was also calculated by the method of Shitara et al (Shitara et al., 2013). K_p is defined as the ratio of the total concentration of compound in cells to total concentration in media at steady state. In this approach the inverse of the K_p at 4°C is considered to be equal to the fraction unbound in cells. Henceforth, this method will be referred to as the "steady state method".

Predictive ability of the two-compartment model

The bias of the predictions and the scatter associated with the predictions were assessed from the average fold error (AFE), and absolute average fold error (AAFE) respectively, and are shown in equations 9 and 10.

$$\mathrm{AFE} = 10^{\frac{1}{n}\sum \log \frac{\mathrm{Predicted}}{\mathrm{Observed}}} \quad \ldots\ldots\ldots\ldots\ldots\ldots 9$$

$$\mathrm{AAFE} = 10^{\frac{1}{n}\sum \log \frac{|\mathrm{Predicted}|}{|\mathrm{Observed}|}} \quad \ldots\ldots\ldots\ldots\ldots\ldots 10$$

Determinations of fraction transported (f_t) by a particular transporter

As mentioned previously, the hepatocyte model (equations 6 and 7) accounted for multiple hepatic disposition processes of pitavastatin. The hepatocyte accumulation of pitavastatin due to each individual process ($CL_{passive}$ or $CL_{uptake\ transporter}$) was simulated, one at a time, and the area under the curve (AUC) of each individual process was calculated by non-compartmental analysis. AUC values of the individual processes (passive diffusion, OATP1B1, OATP1B3, and NTCP) were added to obtain a total simulated AUC. Of note, total simulated AUC values were similar to observed AUC values. Subsequently, AUC of each individual process was expressed as a fraction of the total simulated AUC to obtain the f_t. Initial simulations showed MRP3 to have

DMD Fast Forward. Published on April 17, 2018 as DOI: 10.1124/dmd.118.080614
This article has not been copyedited and formatted. The final version may differ from this version.

minimal impact on hepatocyte disposition. Thus, MRP3 was not considered in the final f_t calculations.

IVIVC of inhibition of uptake of pitavastatin

IVIVCs of inhibition of uptake were determined from the Rowland-Matin equation (Equation 11), which is a method of estimating the fold change in exposure due to inhibition of a particular elimination pathway (in this case transporters) by a particular inhibitor. This equation/approach has been employed previously for calculating AUC fold changes resulting from hepatic uptake inhibition (Elsby et al., 2012; Shen et al., 2013).

$$AUCR = \frac{AUC_i}{AUC_c} = \frac{1}{\sum_{i=1}^{n} \frac{f_t f_h}{1+[I]/K_i} + (1 - \sum_{i=1}^{n} f_t f_h)} \quad \text{.....11}$$

Where, AUCR is the ratio of AUCs obtained in the presence and absence of an inhibitor. AUC_i and AUC_c are the AUC in the presence or absence of an inhibitor, respectively, f_t is the fraction transported, K_i is the reversible inhibition constant. [I] is the in vivo concentration of the inhibitor, and for this parameter, unbound hepatic inlet concentration ($[I]_{u,inlet,max}$) was considered. K_i values and physicochemical properties/PK parameters used for calculating $[I]_{u,inlet,max}$ were obtained from the literature and are provided in the supplementary section (Table S3).

In equation 9, f_h is the fraction of pitavastatin eliminated by the liver. The fraction of pitavastatin eliminated in urine as unchanged pitavastatin is 3% (as provided in the label of Liavlo®) (Label of Liavlo). Thus f_h was estimated to be 0.97. Of note, renal clearance of pitavastatin is often considered to be 0 (Varma et al., 2014; Riede et al., 2016), and hence the value of 0.97 is a reasonable estimation of f_h of pitavastatin.

DMD Fast Forward. Published on April 17, 2018 as DOI: 10.1124/dmd.118.080614
This article has not been copyedited and formatted. The final version may differ from this version.

Results

Uptake of E3S, CCK-8, TCA, and pitavastatin in HEK293-transfected cells

Concentration dependent uptake of E3S, CCK-8, and TCA were evaluated in HEK293 cells transfected with OATP1B1, OATP1B3, and NTCP, respectively. Total, passive, and active uptake of each substrate is shown in Supplementary figure S1, and the kinetic constants of active uptake are listed in Table 1. As shown in Table 1, the K_m values of all three substrates were similar to what has been reported previously for the corresponding transporter (≤1 μM for high affinity binding of E3S to OATP1B1, 3.8-6.5 μM for CCK-8, and 5.4-22.1 μM for TCA) (Hirano et al., 2004; Leonhardt et al., 2010; Schwarz et al., 2011; DeGorter et al., 2012; Sharma et al., 2012; De Bruyn et al., 2014; Gozalpour et al., 2014; Marada et al., 2015).

The concentration dependent uptake of pitavastatin was also evaluated. Values describing the total, passive, and active uptake of pitavastatin are shown in Supplementary figure S1, and the kinetic constants of active uptake are listed in Table 1. As shown in Table 1, the K_m values of pitavastatin for OATP1B1, OATP1B3, and NTCP in this study were similar to previously reported values (0.8-4.8 μM for OATP1B1, 2.6-3.3 μM for OATP1B3, and 38.5 μM for NTCP) (Hirano et al., 2004; Sharma et al., 2012; Soars et al., 2012; Izumi et al., 2015; Vildhede et al., 2016).

Uptake of E3S, CCK-8, and TCA in hepatocytes, and estimation of RAF values

Concentration-dependent uptake of E3S, CCK-8, and TCA in suspension and sandwich culture hepatocytes was evaluated. For E3S, passive diffusion was estimated at 4°C, and also at 37°C in the presence of 100 μM rifamycin SV. There was no appreciable difference in passive uptake of E3S between these two approaches. Hence for CCK-8 and TCA, incubations at 4°C only were used for estimating passive diffusion.

DMD Fast Forward. Published on April 17, 2018 as DOI: 10.1124/dmd.118.080614
This article has not been copyedited and formatted. The final version may differ from this version.

Total, passive, and active uptake of each substrate are shown in Supplementary Figures S2 and S3, while the kinetic constants of active uptake are listed in Table 2. Of note, the K_m values of E3S, CCK-8, and TCA obtained using hepatocytes were similar to the values determined in HEK293 cells.

The relative activity factors (RAFs) of OATP1B1, OATP1B3, and NTCP between transfected HEK293 cells and hepatocytes are listed in Table 2. The RAF values indicated that the activity of OATP1B1 in hepatocytes was similar to that in the transfected cells. The activities of OATP1B3 and NTCP in hepatocytes were much lower than in transfected cells, and this was especially evident in lots HUP1001 and HU1651 for OATP1B3. In lot HUM4122D, the RAF values also indicated that in SCHH compared with suspensions, OATP1B1 activity decreased by 2.4X, OATP1B3 activity remained constant, and the NTCP activity increased by 2X.

Modeling of hepatocyte uptake of pitavastatin at 4°C to derive $CL_{passive}$ and $f_{u,cell}$

Time-dependent uptake of pitavastatin at 4°C in hepatocytes was fitted to the two-compartment model (equations 6 and 7) to derive $CL_{passive}$ and $f_{u,cell}$. The fits to the uptake data at 4°C are shown in Figure 1, and the derived values of $CL_{passive}$ and $f_{u,cell}$ are listed in Table 3. Additionally, $f_{u,cell}$ estimates from the steady state method, which is a more commonly employed method of $f_{u,cell}$ determination, are also reported in Table 3 (Shitara et al., 2013). Estimates of $f_{u,cell}$ by the steady state approach were found to be very similar to those determined by modeling, indicating the modeling approach to be able to generate reliable $f_{u,cell}$ estimates, at least for pitavastatin .

Prediction of the hepatocyte uptake of pitavastatin at 37°C and determination of f_t

Time-dependent uptake of pitavastatin at 37°C in hepatocytes was predicted by the two-compartment model (equations 6 and 7). For the predictions, all model parameters were

DMD Fast Forward. Published on April 17, 2018 as DOI: 10.1124/dmd.118.080614
This article has not been copyedited and formatted. The final version may differ from this version.

incorporated as fixed parameters and none of the parameters were fitted. $CL_{passive}$ and $f_{u,cell}$ derived from modeling of 4°C uptake data were used for the 37°C predictions, along with the V_{max} and K_m of each transporter as predicted using the RAF method.

Predictions of time-dependent uptake of pitavastatin in hepatocytes at 37°C are shown in Figure 2. The AFE values were close to unity indicating there to be no bias for either over-prediction or under-prediction of pitavastatin disposition in both cells and medium. The AAFE values were < 1.25 indicating low scatter. The goodness of fit also indicated that RAF values had been correctly estimated, and also that $CL_{passive}$ and $f_{u,cell}$ derived from 4°C incubations are suitable representatives of those parameters at 37°C for pitavastatin. Overall, there was good predictive ability in both suspension and SCHH format of hepatocytes.

Hepatocyte disposition processes that were modeled for pitavastatin were uptake, bidirectional passive diffusion, basolateral efflux by MRP3, and intracellular binding. As mentioned above, for MRP3 due to unavailability of a selective MRP3 RAF probe substrate, previously published K_m (448 µM) and REF estimates were used (Vildhede et al., 2016). Initial simulations showed MRP3 to have minimal impact on hepatocyte disposition (Supplementary Table S2). Simulations showed that the V_{max} of MRP3 would need to be considerably higher ($\geq 10^4$ X) than the currently used V_{max} to substantially affect cellular accumulation of pitavastatin. From this analysis it was judged that MRP3 would have minimal impact on intracellular concentrations of pitavastatin. Thus MRP3 was not considered in the final f_t calculations.

For all other processes (transporter and passive diffusion), the f_t values of pitavastatin were estimated and indicated the rank order of contributions to hepatocyte uptake of pitavastatin to be OATP1B1>passive diffusion> NTCP ≥OATP1B3 (Table 4). In suspension and SCHH formats, f_t

DMD Fast Forward. Published on April 17, 2018 as DOI: 10.1124/dmd.118.080614
This article has not been copyedited and formatted. The final version may differ from this version.

of OATP1B1 was approximately 0.6 and 0.5, respectively. In lot HUM4122D, which was the only lot used in both culture formats, there was a 1.3X decrease in OATP1B1 contribution in SCHH compared with suspensions, which was lesser than that indicated by RAF estimates alone (2.4X). A significant portion of the total hepatocyte uptake of pitavastatin was by passive diffusion (~30 % in both culture formats). Thus the actual reduction of OATP1B1 f_t in SCHH compared with suspensions, was less pronounced than that indicated by RAF estimates alone. In both culture formats, OATP1B3 constituted < 10% of total uptake. NTCP contributed <10% of the total uptake in suspensions and slightly greater than 10% of the total uptake in SCHH.

IVIVC of inhibition of pitavastatin uptake

IVIVCs of hepatic uptake inhibition of pitavastatin were estimated for two commonly used OATP inhibitors, rifampicin and cyclosporine. PBPK modeling of clinical PK data of several OATP substrates has shown that in vitro K_i values are insufficient in recovering clinical PK profiles of these compounds and when used in PBPK models resulted in significant under-predictions of exposure changes in the presence of inhibitors. The general opinion of these studies is that for rifampicin and cyclosporine, in vitro K_i values are lower than the corresponding in vivo K_i values. Subsequently in these studies, model-optimized K_i values, referred to as in vivo K_i values, led to much improved recovery of PK data (Varma et al., 2012; Jamei et al., 2014; Duan et al., 2016; Yoshikado et al., 2016). Rifampicin and cyclosporine each have in vivo K_i values reported in the literature, and therefore these values were employed for estimating AUCRs of hepatic uptake inhibition in this study. The in vivo K_i values of cyclosporine for inhibition of OATP1B1, OATP1B3, and NTCP are provided in Supplementary Table S3 (Jamei et al., 2014). For rifampicin, it was reported in an article published from FDA that in vivo K_i of OATP1B1 and OATP1B3 inhibition are at least $1/10^{th}$ of the in vitro values of

DMD Fast Forward. Published on April 17, 2018 as DOI: 10.1124/dmd.118.080614
This article has not been copyedited and formatted. The final version may differ from this version.

0.9 µM and 0.3 µM (Duan et al., 2016). Thus rifampicin K_i values for OATP1B1 and OATP1B3 were considered to be 0.09 µM and 0.03 µM respectively. For NTCP inhibition by rifampicin, the in vitro K_i values (138.5 µM) was used due to lack of information regarding in vivo K_i values.

The predicted AUCRs of hepatic uptake inhibition of pitavastatin (calculated from Equation 11) are listed in Table 5**.** In vivo, AUC of pitavastatin increased by 5.1-6.7X in the presence of rifampicin and by 4.6X in the presence of cyclosporine (Chen et al., 2013; Prueksaritanont et al., 2014; Kim et al., 2016). The rifampicin studies were conducted in three different populations, and in this study, the AUC exposure change observed in the Caucasian population (5.8X) was considered to be the benchmark for IVIVCs of hepatic inhibition with rifampicin (Prueksaritanont et al., 2014). It was found that predicted AUCRs under-predicted observed AUCRs (0.33-0.51X for rifampicin and 0.41-0.54X for cyclosporine). The under-predictions were not surprising, as it has been shown for many OATP substrates that in vitro hepatic uptake clearance is usually much lower than in vivo hepatic uptake clearance (Jones et al., 2012; Menochet et al., 2012b; Varma et al., 2012; Li et al., 2014; Varma et al., 2014). This discrepancy is thought to be due to transporter activity differences between in vitro models and liver tissue. For purposes of PBPK modeling or IVIVCs of hepatic uptake, a way of resolving this discrepancy has been the application of SFs to in vitro uptake clearance. We used a similar approach and applied empirical SFs to the RAF values. Subsequently, hepatocyte uptake of pitavastatin was re-simulated and f_t values were re-estimated. It was observed that SFs of 10-15 resulted in projected AUCRs being within 0.8-1.05X of in vivo AUCRs (Table 5)**.**

DMD Fast Forward. Published on April 17, 2018 as DOI: 10.1124/dmd.118.080614
This article has not been copyedited and formatted. The final version may differ from this version.

Discussion

From a DDI perspective, f_t is a valuable parameter in helping refine DDI predictions made through either static equations or PBPK modeling. RAF methods have previously been used for estimating f_t; however these estimations have typically described a static process rather than considering the transport of a compound over time. In cases where RAF approaches have been used in a dynamic manner, the data obtained in transfected cells were not translated to a more holistic model (Mathialagan et al., 2017). The goal of this study was to supplement in vitro RAF data with modeling techniques that allow integration of processes in addition to uptake in order to predict cellular accumulation in a more holistic model (hepatocytes), and subsequently determine a more accurate f_t value for individual transporters as part of a dynamic process. This should increase the predictive ability of interactions associated with individual transporters, and allow identification of transporter(s) at which DDIs would be most significant.

Pitavastatin was selected as the probe substrate since its metabolic clearance and biliary clearance are low in comparison to uptake clearance (Watanabe et al., 2010; Varma et al., 2014; Riede et al., 2016; Vildhede et al., 2016). Hepatocyte disposition processes that were modeled for pitavastatin were uptake, bidirectional passive diffusion, basolateral efflux by MRP3, and intracellular binding. Quantification of hepatocyte uptake of pitavastatin by the DRF approach indicated the primary determinant of pitavastatin hepatocyte uptake to be OATP1B1 (f_t = 0.48-0.66 based upon total uptake) with minor contributions from OATP1B3 and NTCP (f_t = 0.01-0.09 and 0.02-0.13, respectively). The f_t values correlate well with what is known about the in vivo hepatic uptake of pitavastatin i.e. it is mediated primarily through OATP1B1 (Prueksaritanont et al., 2014). Thus the DRF approach was able to correctly identify the

DMD Fast Forward. Published on April 17, 2018 as DOI: 10.1124/dmd.118.080614
This article has not been copyedited and formatted. The final version may differ from this version.

transporter with the largest uptake contribution. This information may not have been as easily gleaned from studies done in transfected cells alone, where pitavastatin had similar transport efficiencies (V_{max}/K_m) for OATP1B1, OATP1B3, and NTCP (Table 1). Of note, MRP3 had minimal impact on pitavastatin hepatocyte accumulation. This result was logical since MRP3 transports pitavastatin with a much lower affinity compared to OATPs and also has a much lower hepatic expression.

In previous studies, static RAF or chemical inhibition approaches have estimated transporter contributions towards hepatocyte uptake of pitavastatin to be 42-95%, 1.8-12.3%, and 29% for OATP1B1, OATP1B3, and NTCP, respectively (Hirano et al., 2004; Bi et al., 2012; Kunze et al., 2014) . Some of these studies estimated transporter contributions based upon active uptake alone, thus resulting in artificially high f_t values. More recently, a dynamic REF-based method estimated the f_t of OATP1B1 and NTCP to be 57%-87% and 6-22%, respectively (Vildhede et al., 2016). We were interested in evaluating if an approach similar to that of Vildhede et al., but using translations based upon activities instead of expression, is able to simulate hepatocyte disposition. The f_t values obtained from our DRF approach (48-66%, 1-9%, and 2-17% for OATP1B1, OATP1B3, and NTCP, respectively) indicated this approach to be able to produce results at par with other methods.

We subsequently employed the f_t values to determine the in vitro to in vivo predictive ability of hepatic uptake inhibition of pitavastatin. Incidentally, such pieces of information are of high value to clinical teams. AUC changes of a compound resulting from hepatic uptake inhibition have previously been estimated using either the Rowland Matin equation (Elsby et al., 2012;

Shen et al., 2013) or the extended clearance concept (Varma et al., 2014). Here, we utilized the former approach (equation 11). Inhibitors considered were rifampicin and cyclosporine due to the wealth of clinical data available for these compounds. It was found that AUCR predictions were 0.4X of observations in suspensions and 0.5X in SCHH**.** Back-calculations showed that in order for the predicted AUCRs to be exactly the same as observed AUCRs, active uptake would have to account for 80-88% of total uptake into hepatocytes. In comparison, the hepatocyte lots used in this study showed 65-70% active uptake**,** which lead to the 2-2.5X under-predictions of hepatic uptake inhibition.

The lower-than-optimal percentage of active uptake in hepatocytes may be due to a decrease in transporter activities in hepatocytes compared to liver tissue. For many OATP1B1/1B3 substrates, in vitro hepatic uptake clearances are seen to be significantly lower than in vivo uptake clearances (Watanabe et al., 2010; Jones et al., 2012; Menochet et al., 2012b; Varma et al., 2012; Li et al., 2014; Varma et al., 2014). For all of these OATP substrates, application of empirical SFs to in vitro uptake clearances resulted in improved IVIVCs. The SFs are hypothesized to represent activity differences between hepatocytes and liver tissue (Varma et al., 2014). Thus, in our study, following the 2-2.5X under-predictions of hepatic uptake inhibition, SFs were incorporated into the RAF estimates of each transporter and the effect on IVIVCs was re-evaluated. Simulations suggested that SFs of 10-15 resulted in the desired percentage of active uptake (80-88%) and subsequently provided projected AUCRs that were the same as observed AUCRs **(**Table 5**).** Thus while experimentally determined RAF values allowed accurate translation from transfected cells to hepatocytes, SFs were required for bridging the presumable activity differences between hepatocytes and liver. For accurate IVIVCs of hepatic uptake

DMD Fast Forward. Published on April 17, 2018 as DOI: 10.1124/dmd.118.080614
This article has not been copyedited and formatted. The final version may differ from this version.

inhibition of NCEs, we suggest calibration of hepatocytes with prototypical OATP substrates and inhibitors to determine system-specific SFs, which could subsequently be applied towards IVIVCs of hepatic uptake inhibition of the NCE with prototypical OATP inhibitors. However, SFs of OATP substrates exhibit a wide range of values and thus a SF that works for one particular probe substrate may not be suitable for a new NCE. While this is admittedly a limitation, selection of a probe substrate with similar active and passive uptake properties as the NCE would be a logical approach for determination of system-specific SFs. A road map of the DRF approach is provided in Figure 3.

Pitavastatin has similar in vitro efficiency (V_{max}/K_m) for OATP1B1 and OATP1B3 (Table 1); however the f_t of the two transporters were remarkably different (OATP1B3 <0.1, OATP1B1 ~ 0.48-0.66). We explored the possible reasons for this difference by researching the relative expression of these transporters. Protein expression ratio of OATP1B3:OATP1B1 is 0.4-0.9:1 in liver tissue and 0.14-0.43:1 in hepatocytes (Badee et al., 2015; Peng et al., 2015; Burt et al., 2016; Prasad et al., 2016). If the in vitro efficiencies of pitavastatin in transfected cells are translated to hepatocyte clearance based upon hepatocyte protein expression (assuming that functional activity is directly related to transporter abundance), then hepatocyte clearance of OATP1B3 should be 0.1-0.3X that of OATP1B1. Our results however indicated that OATP1B3 clearance was 0.02-0.03X of OATP1B1 clearance. As such, the RAF approach indicated the activity of OATP1B3 in comparison to OATP1B1 activity to be much less than what would have been expected if transporter expression and activity had a 1:1 correlation. While it is not easy to decipher the reason for this lack of correlation, in most of the protein quantitation studies cited above, protein expression was determined in crude membrane fractions, which presumably will have more

protein than that present in plasma membrane fractions alone (Kunze et al., 2014). Further research on plasma membrane quantitation of OATP proteins and on alternative specific substrates of OATP1B3 might shed more light on the extent of correlation between abundance and activities in hepatocytes.

The RAF approach is based upon the assumption that probe substrates are selective for the transporters. This is a limitation, since compounds are typically substrates of multiple transporters. However, a way around this limitation may be utilization of probe substrate concentrations that are selective for a particular transporter. For example, E3S has been used as a selective substrate of OATP1B1 for RAF purposes (Hirano et al., 2004; Kunze et al., 2014), but it is a substrate of OATP2B1 and NTCP as well. We found E3S to be a higher affinity substrate of OATP1B1 (K_m = 0.5µM), compared to OATP2B1 (K_m = 20.2 µM) and NTCP (K_m=20.6 µM). Further, E3S clearances in HEK293-OATP2B1 and HEK293-NTCP cells were only ~20-25% of the clearance in HEK293-OATP1B1 cells (data not shown). Thus, we assumed that at low concentrations (< 5µM), E3S can offer selectivity for OATP1B1. In retrospect, this assumption was a valid one to make since there was generally good agreement between observed and predicted hepatocyte uptake of pitavastatin.

In summary, this is the first study to amalgamate in vitro RAF data with modeling techniques that allow integration of multiple processes to estimate f_t of hepatic uptake. For pitavastatin, a compound with a minor metabolic component of clearance and where hepatic disposition is uptake-limited, the transporter contributions were correctly estimated by this technique. Future studies will evaluate the utility of this approach for f_t estimations of compounds for which

metabolic and/or biliary clearance are also substantial in relation to uptake clearance. Further, OATP1B1 polymorphisms are known to affect pitavastatin exposure significantly in certain ethnicities. Predicting such changes would be another potential application of the DRF approach.

Acknowledgements

The authors would like to thank Dr. Timothy Tracy for his careful and constructive review of this manuscript.

Authorship contributions

Participated in research design: Mitra, Weinheimer, Taub.

Conducted experiments: Weinheimer, Mitra.

Performed data analysis: Mitra, Weinheimer.

Wrote or contributed to the writing of the manuscript: Mitra, Michalewicz, Weinheimer, Taub.

References

Badee J, Achour B, Rostami-Hodjegan A, and Galetin A (2015) Meta-analysis of expression of hepatic organic anion-transporting polypeptide (OATP) transporters in cellular systems relative to human liver tissue. *Drug Metab Dispos* **43:**424-432.

Bi YA, Kimoto E, Sevidal S, Jones HM, Barton HA, Kempshall S, Whalen KM, Zhang H, Ji C, Fenner KS, El-Kattan AF, and Lai Y (2012) In vitro evaluation of hepatic transporter-mediated clinical drug-drug interactions: hepatocyte model optimization and retrospective investigation. *Drug Metab Dispos* **40:**1085-1092.

Bi YA, Qiu X, Rotter CJ, Kimoto E, Piotrowski M, Varma MV, Ei-Kattan AF, and Lai Y (2013) Quantitative assessment of the contribution of sodium-dependent taurocholate co-transporting polypeptide (NTCP) to the hepatic uptake of rosuvastatin, pitavastatin and fluvastatin. *Biopharm Drug Dispos* **34:**452-461.

Burt HJ, Riedmaier AE, Harwood MD, Crewe HK, Gill KL, and Neuhoff S (2016) Abundance of Hepatic Transporters in Caucasians: A Meta-Analysis. *Drug Metab Dispos* **44:**1550-1561.

Chapy H, Klieber S, Brun P, Gerbal-Chaloin S, Boulenc X, and Nicolas O (2015) PBPK modeling of irbesartan: incorporation of hepatic uptake. *Biopharm Drug Dispos* **36:**491-506.

Chen Y, Zhang W, Huang WH, Tan ZR, Wang YC, Huang X, and Zhou HH (2013) Effect of a single-dose rifampin on the pharmacokinetics of pitavastatin in healthy volunteers. *Eur J Clin Pharmacol* **69:**1933-1938.

De Bruyn T, Sempels W, Snoeys J, Holmstock N, Chatterjee S, Stieger B, Augustijns P, Hofkens J, Mizuno H, and Annaert P (2014) Confocal imaging with a fluorescent bile acid

analogue closely mimicking hepatic taurocholate disposition. *J Pharm Sci* **103:**1872-1881.

DeGorter MK, Ho RH, Leake BF, Tirona RG, and Kim RB (2012) Interaction of three regiospecific amino acid residues is required for OATP1B1 gain of OATP1B3 substrate specificity. *Mol Pharm* **9:**986-995.

Duan P, Zhao P, and Zhang L (2016) Physiologically Based Pharmacokinetic (PBPK) Modeling of Pitavastatin and Atorvastatin to Predict Drug-Drug Interactions (DDIs). *Eur J Drug Metab Pharmacokinet*.

Elsby R, Hilgendorf C, and Fenner K (2012) Understanding the critical disposition pathways of statins to assess drug-drug interaction risk during drug development: it's not just about OATP1B1. *Clin Pharmacol Ther* **92:**584-598.

Gozalpour E, Greupink R, Wortelboer HM, Bilos A, Schreurs M, Russel FG, and Koenderink JB (2014) Interaction of digitalis-like compounds with liver uptake transporters NTCP, OATP1B1, and OATP1B3. *Mol Pharm* **11:**1844-1855.

Hirano M, Maeda K, Shitara Y, and Sugiyama Y (2004) Contribution of OATP2 (OATP1B1) and OATP8 (OATP1B3) to the hepatic uptake of pitavastatin in humans. *J Pharmacol Exp Ther* **311:**139-146.

Izumi S, Nozaki Y, Maeda K, Komori T, Takenaka O, Kusuhara H, and Sugiyama Y (2015) Investigation of the impact of substrate selection on in vitro organic anion transporting polypeptide 1B1 inhibition profiles for the prediction of drug-drug interactions. *Drug Metab Dispos* **43:**235-247.

Jamei M, Bajot F, Neuhoff S, Barter Z, Yang J, Rostami-Hodjegan A, and Rowland-Yeo K (2014) A mechanistic framework for in vitro-in vivo extrapolation of liver membrane

transporters: prediction of drug-drug interaction between rosuvastatin and cyclosporine. *Clin Pharmacokinet* **53:**73-87.

Jigorel E and Houston JB (2012) Utility of drug depletion-time profiles in isolated hepatocytes for accessing hepatic uptake clearance: identifying rate-limiting steps and role of passive processes. *Drug Metab Dispos* **40:**1596-1602.

Jones HM, Barton HA, Lai Y, Bi YA, Kimoto E, Kempshall S, Tate SC, El-Kattan A, Houston JB, Galetin A, and Fenner KS (2012) Mechanistic pharmacokinetic modeling for the prediction of transporter-mediated disposition in humans from sandwich culture human hepatocyte data. *Drug Metab Dispos* **40:**1007-1017.

Kim SJ, Yoshikado T, Ieiri I, Maeda K, Kimura M, Irie S, Kusuhara H, and Sugiyama Y (2016) Clarification of the Mechanism of Clopidogrel-Mediated Drug-Drug Interaction in a Clinical Cassette Small-dose Study and Its Prediction Based on In Vitro Information. *Drug Metab Dispos* **44:**1622-1632.

Kimoto E, Yoshida K, Balogh LM, Bi YA, Maeda K, El-Kattan A, Sugiyama Y, and Lai Y (2012) Characterization of organic anion transporting polypeptide (OATP) expression and its functional contribution to the uptake of substrates in human hepatocytes. *Mol Pharm* **9:**3535-3542.

Kunze A, Huwyler J, Camenisch G, and Poller B (2014) Prediction of organic anion-transporting polypeptide 1B1- and 1B3-mediated hepatic uptake of statins based on transporter protein expression and activity data. *Drug Metab Dispos* **42:**1514-1521.

Label_of_Liavlo https://www.accessdata.fda.gov/scripts/cder/daf/index.cfm?event=overview.process&ApplNo=022363. Accessed March 2018.

Leonhardt M, Keiser M, Oswald S, Kuhn J, Jia J, Grube M, Kroemer HK, Siegmund W, and Weitschies W (2010) Hepatic uptake of the magnetic resonance imaging contrast agent Gd-EOB-DTPA: role of human organic anion transporters. *Drug Metab Dispos* **38:**1024-1028.

Li R, Barton HA, Yates PD, Ghosh A, Wolford AC, Riccardi KA, and Maurer TS (2014) A "middle-out" approach to human pharmacokinetic predictions for OATP substrates using physiologically-based pharmacokinetic modeling. *J Pharmacokinet Pharmacodyn* **41:**197-209.

Lonza_Suspension_and_Plateable_Cryopreserved_Hepatocytes_protocol https://www.lonza.com/products-services/bio-research/adme-tox/hepatocytes-and-media.aspx. Accessed March 2018.

Marada VV, Florl S, Kuhne A, Burckhardt G, and Hagos Y (2015) Interaction of human organic anion transporter polypeptides 1B1 and 1B3 with antineoplastic compounds. *Eur J Med Chem* **92:**723-731.

Mathialagan S, Piotrowski MA, Tess DA, Feng B, Litchfield J, and Varma MV (2017) Quantitative Prediction of Human Renal Clearance and Drug-Drug Interactions of Organic Anion Transporter Substrates Using In Vitro Transport Data: A Relative Activity Factor Approach. *Drug Metab Dispos* **45:**409-417.

Menochet K, Kenworthy KE, Houston JB, and Galetin A (2012a) Simultaneous assessment of uptake and metabolism in rat hepatocytes: a comprehensive mechanistic model. *J Pharmacol Exp Ther* **341:**2-15.

Menochet K, Kenworthy KE, Houston JB, and Galetin A (2012b) Use of mechanistic modeling to assess interindividual variability and interspecies differences in active uptake in human and rat hepatocytes. *Drug Metab Dispos* **40:**1744-1756.

Peng KW, Bacon J, Zheng M, Guo Y, and Wang MZ (2015) Ethnic variability in the expression of hepatic drug transporters: absolute quantification by an optimized targeted quantitative proteomic approach. *Drug Metab Dispos* **43:**1045-1055.

Pfeifer ND, Harris KB, Yan GZ, and Brouwer KL (2013) Determination of intracellular unbound concentrations and subcellular localization of drugs in rat sandwich-cultured hepatocytes compared with liver tissue. *Drug Metab Dispos* **41:**1949-1956.

Prasad B, Gaedigk A, Vrana M, Gaedigk R, Leeder JS, Salphati L, Chu X, Xiao G, Hop C, Evers R, Gan L, and Unadkat JD (2016) Ontogeny of Hepatic Drug Transporters as Quantified by LC-MS/MS Proteomics. *Clin Pharmacol Ther* **100:**362-370.

Prueksaritanont T, Chu X, Evers R, Klopfer SO, Caro L, Kothare PA, Dempsey C, Rasmussen S, Houle R, Chan G, Cai X, Valesky R, Fraser IP, and Stoch SA (2014) Pitavastatin is a more sensitive and selective organic anion-transporting polypeptide 1B clinical probe than rosuvastatin. *Br J Clin Pharmacol* **78:**587-598.

Ramsden D, Tweedie DJ, Chan TS, Taub ME, and Li Y (2014) Bridging in vitro and in vivo metabolism and transport of faldaprevir in human using a novel cocultured human hepatocyte system, HepatoPac. *Drug Metab Dispos* **42:**394-406.

Riede J, Poller B, Umehara K, Huwyler J, and Camenisch G (2016) New IVIVE method for the prediction of total human clearance and relative elimination pathway contributions from in vitro hepatocyte and microsome data. *Eur J Pharm Sci* **86:**96-102.

Schwarz UI, Meyer zu Schwabedissen HE, Tirona RG, Suzuki A, Leake BF, Mokrab Y, Mizuguchi K, Ho RH, and Kim RB (2011) Identification of novel functional organic anion-transporting polypeptide 1B3 polymorphisms and assessment of substrate specificity. *Pharmacogenet Genomics* **21:**103-114.

Sharma P, Butters CJ, Smith V, Elsby R, and Surry D (2012) Prediction of the in vivo OATP1B1-mediated drug-drug interaction potential of an investigational drug against a range of statins. *Eur J Pharm Sci* **47:**244-255.

Shen H, Yang Z, Mintier G, Han YH, Chen C, Balimane P, Jemal M, Zhao W, Zhang R, Kallipatti S, Selvam S, Sukrutharaj S, Krishnamurthy P, Marathe P, and Rodrigues AD (2013) Cynomolgus monkey as a potential model to assess drug interactions involving hepatic organic anion transporting polypeptides: in vitro, in vivo, and in vitro-to-in vivo extrapolation. *J Pharmacol Exp Ther* **344:**673-685.

Shitara Y, Itoh T, Sato H, Li AP, and Sugiyama Y (2003) Inhibition of transporter-mediated hepatic uptake as a mechanism for drug-drug interaction between cerivastatin and cyclosporin A. *J Pharmacol Exp Ther* **304:**610-616.

Shitara Y, Maeda K, Ikejiri K, Yoshida K, Horie T, and Sugiyama Y (2013) Clinical significance of organic anion transporting polypeptides (OATPs) in drug disposition: their roles in hepatic clearance and intestinal absorption. *Biopharm Drug Dispos* **34:**45-78.

Soars MG, Barton P, Ismair M, Jupp R, and Riley RJ (2012) The development, characterization, and application of an OATP1B1 inhibition assay in drug discovery. *Drug Metab Dispos* **40:**1641-1648.

Stoscheck CM (1990) Quantitation of protein. *Methods Enzymol* **182:**50-68.

Taub ME, Mease K, Sane RS, Watson CA, Chen L, Ellens H, Hirakawa B, Reyner EL, Jani M, and Lee CA (2011) Digoxin is not a substrate for organic anion-transporting polypeptide transporters OATP1A2, OATP1B1, OATP1B3, and OATP2B1 but is a substrate for a sodium-dependent transporter expressed in HEK293 cells. *Drug Metab Dispos* **39:**2093-2102.

Varma MV, Bi YA, Kimoto E, and Lin J (2014) Quantitative prediction of transporter- and enzyme-mediated clinical drug-drug interactions of organic anion-transporting polypeptide 1B1 substrates using a mechanistic net-effect model. *J Pharmacol Exp Ther* **351:**214-223.

Varma MV, Lai Y, Feng B, Litchfield J, Goosen TC, and Bergman A (2012) Physiologically based modeling of pravastatin transporter-mediated hepatobiliary disposition and drug-drug interactions. *Pharm Res* **29:**2860-2873.

Vildhede A, Mateus A, Khan EK, Lai Y, Karlgren M, Artursson P, and Kjellsson MC (2016) Mechanistic Modeling of Pitavastatin Disposition in Sandwich-Cultured Human Hepatocytes: A Proteomics-Informed Bottom-Up Approach. *Drug Metab Dispos* **44:**505-516.

Watanabe T, Kusuhara H, Maeda K, Kanamaru H, Saito Y, Hu Z, and Sugiyama Y (2010) Investigation of the rate-determining process in the hepatic elimination of HMG-CoA reductase inhibitors in rats and humans. *Drug Metab Dispos* **38:**215-222.

Williamson B, Soars AC, Owen A, White P, Riley RJ, and Soars MG (2013) Dissecting the relative contribution of OATP1B1-mediated uptake of xenobiotics into human hepatocytes using siRNA. *Xenobiotica* **43:**920-931.

Yoshikado T, Yoshida K, Kotani N, Nakada T, Asaumi R, Toshimoto K, Maeda K, Kusuhara H, and Sugiyama Y (2016) Quantitative Analyses of Hepatic OATP-Mediated Interactions Between Statins and Inhibitors Using PBPK Modeling With a Parameter Optimization Method. *Clin Pharmacol Ther* **100:**513-523.

Footnotes

This research was funded by Boehringer-Ingelheim Pharmaceuticals, Inc.

Figure legends

Fig. 1: Fitting of the time dependent hepatocyte uptake of pitavastatin at 4°C as represented by media (A1- C1) and intracellular (A2 -C2) concentrations. Open circles represent observed data (individual values), solid lines represent simulations. A1, A2: suspension, lot HUM4122D; B1, B2: SCHH lot HUM4122D; C1, C2: SCHH lot Hu1651.

Fig. 2: Predictions of the time dependent hepatocyte uptake of pitavastatin at 37°C as represented by media (A1-D1) and intracellular (A2-D2) concentrations. Open circles represent observed data (individual values), solid lines represent simulations. A1, A2: suspension, lot HUP1001; B1, B2: suspension, lot HUM4122D; C1, C2: SCHH lot HUM4122D; D1, D2: SCHH lot Hu1651.

Fig. 3: Road map of predicting in vivo exposure changes of a NCE that is a hepatic uptake transporter substrate by the dynamic RAF (DRF) approach.

DMD Fast Forward. Published on April 17, 2018 as DOI: 10.1124/dmd.118.080614
This article has not been copyedited and formatted. The final version may differ from this version.

Tables

Table 1. Kinetic parameters of active uptake of transporter substrates and pitavastatin in transfected HEK293 cells. Each experiment was done twice except the taurocholic acid uptake experiment in HEK293-NTCP, which was done once.

Substrate	Cell type	K_m (μM)	V_{max} (pmol/min/mg)	V_{max}/K_m (μL/min/mg)
Estrone-3-sulfate	HEK293-OATP1B1	0.52 ± 0.03	45.4 ± 0	87.7
CCK-8	HEK293-OATP1B3	3.1 ± 0.7	55.1 ± 16.5	19.0
Taurocholic acid	HEK293-NTCP	14.9	1191	79.9
Pitavastatin	HEK293-OATP1B1	4.2 ± 0.1	187.2 ± 32.5	44.4 ± 6.7
	HEK293-OATP1B3	2.2 ± 0.1	74.2 ± 37.8	32.6 ± 14.8
	HEK293-NTCP	24.3 ± 3.1	866 ± 283	35.2 ± 7.1

Table 2. Kinetic parameters of active uptake of transporter substrates in hepatocytes in suspension or sandwich culture (SCHH). Each experiment was done once except the HUM4122D rifamycin SV experiments that were done twice.

Substrate	Hepatocyte format	Hepatocyte Lot	K_m (μM)	V_{max} (pmol/min/mg)	V_{max}/K_m (μL/min/mg)	RAF
Estrone-3-sulfate	Suspension	HUP1001	1.14	77.63	67.9	0.68
		HUP1001 (rifamycin SV)	0.93	166.2	179.3	1.95
		HUM122D	0.53	114.8	218.2	2.43
		HUM4122D (rifamycin SV)	0.32 ± 0.032	84.4 ± 6.5	269 ± 48	3.02 ± 0.55
	SCHH	HU1651	0.7	84.8	121	1.16
		HUM4122D	1.25	141.8	113.1	1.18
		HUM4122D (rifamycin SV)	0.52	56	108	1.12
CCK-8	Suspension	HUP1001	NC[a]	NC	0.71[b]	0.04
		HUM122D	1.2	6.8	5.8	0.31
	SCHH	HU1651	1.9	3.0	1.6	0.09
		HUM4122D	1.3	7.6	5.9	0.31
Taurocholic acid	Suspension	HUP1001	23.6	437	18.5	0.23
		HUM122D	21.4	246	11.5	0.14
	SCHH	HU1651	12.9	594.3	45.9	0.57
		HUM4122D	25.6	577.1	22.6	0.28

[a] Not calculated due to low active uptake;

[b] Clearance averaged from concentrations where uptake at 37°C>uptake at 4°C.

DMD Fast Forward. Published on April 17, 2018 as DOI: 10.1124/dmd.118.080614
This article has not been copyedited and formatted. The final version may differ from this version.

Table 3. Derivation of passive diffusion clearance ($CL_{passive}$) and fraction unbound in cells ($f_{u,cell}$) from hepatocyte uptake of pitavastatin at 4°C

Hepatocyte lot and culture format	$CL_{passive}$, (CV%) µL/min/mg	$f_{u,cell}$ modeled (CV%)	$f_{u,cell}$ steady state method
HUM4122D (SCHH)	23.8 (8.1 %)	0.015 (5.5 %)	0.017
Hu1651 (SCHH)	29.5 (21 %)	0.020 (10.3 %)	0.019
HUM4122D (suspension)	28.6 (6.95 %)	0.025 (4.9 %)	0.025
HUP1001 (suspension)	29.5[a]	NC[b]	0.026

[a] Experimentally determined, not modeled

[b] Not calculated as the $CL_{passive}$ in lot HUP1001was experimentally determined

DMD Fast Forward. Published on April 17, 2018 as DOI: 10.1124/dmd.118.080614
This article has not been copyedited and formatted. The final version may differ from this version.

Table 4. Contributions of hepatic uptake transporters towards uptake of pitavastatin in hepatocytes

Hepatocyte lot & culture format	Transporter	Fraction of pitavastatin transported (f_t)
HUM4122D (SCHH)	OATP1B1	0.53
	OATP1B3	0.09
	NTCP	0.09
	Passive diffusion	0.30
Hu 1651 (SCHH)	OATP1B1	0.48
	OATP1B3	0.03
	NTCP	0.17
	Passive diffusion	0.32
HUP1001 (suspension)	OATP1B1	0.56
	OATP1B3	0.01
	NTCP	0.07
	Passive diffusion	0.37
HUM4122D (suspension)	OATP1B1	0.66
	OATP1B3	0.03
	NTCP	0.02
	Passive diffusion	0.29

DMD Fast Forward. Published on April 17, 2018 as DOI: 10.1124/dmd.118.080614
This article has not been copyedited and formatted. The final version may differ from this version.

Table 5. IVIVC of inhibition of hepatocyte uptake of pitavastatin

	AUCR with pitavastatin as the substrate drug in the presence of inhibitor drugs	
	Rifampicin	**Cyclosporine**
Observed in vivo AUCR	**5.8**[a]	**4.6**[b]
Predicted AUCRs		
HUM4122D (SCHH)	2.4	2.2
Hu 1651 (SCHH)	1.9	1.9
HUM4122D (suspension)	2.9	2.5
HUP1001 (suspension)	2.2	2
Simulated AUCRs (RAF of each transporter was multiplied by a SF)		
SF =10	5.3	4
SF = 15	5.8	4.2

[a] AUCR of pitavastatin in the presence of rifampicin is 5.1-6.7 based upon data from three studies conducted across three different populations. The AUCR of 5.8 was observed in the Caucasian population and was considered to be the benchmark in this study (Prueksaritanont et al., 2014).

[b] AUCR of pitavastatin in the presence of cyclosporine is based upon data provided in the label of Liavlo® (can be accessed on the FDA website).

DMD Fast Forward. Published on April 17, 2018 as DOI: 10.1124/dmd.118.080614
This article has not been copyedited and formatted. The final version may differ from this version.

Figures

Figure 1

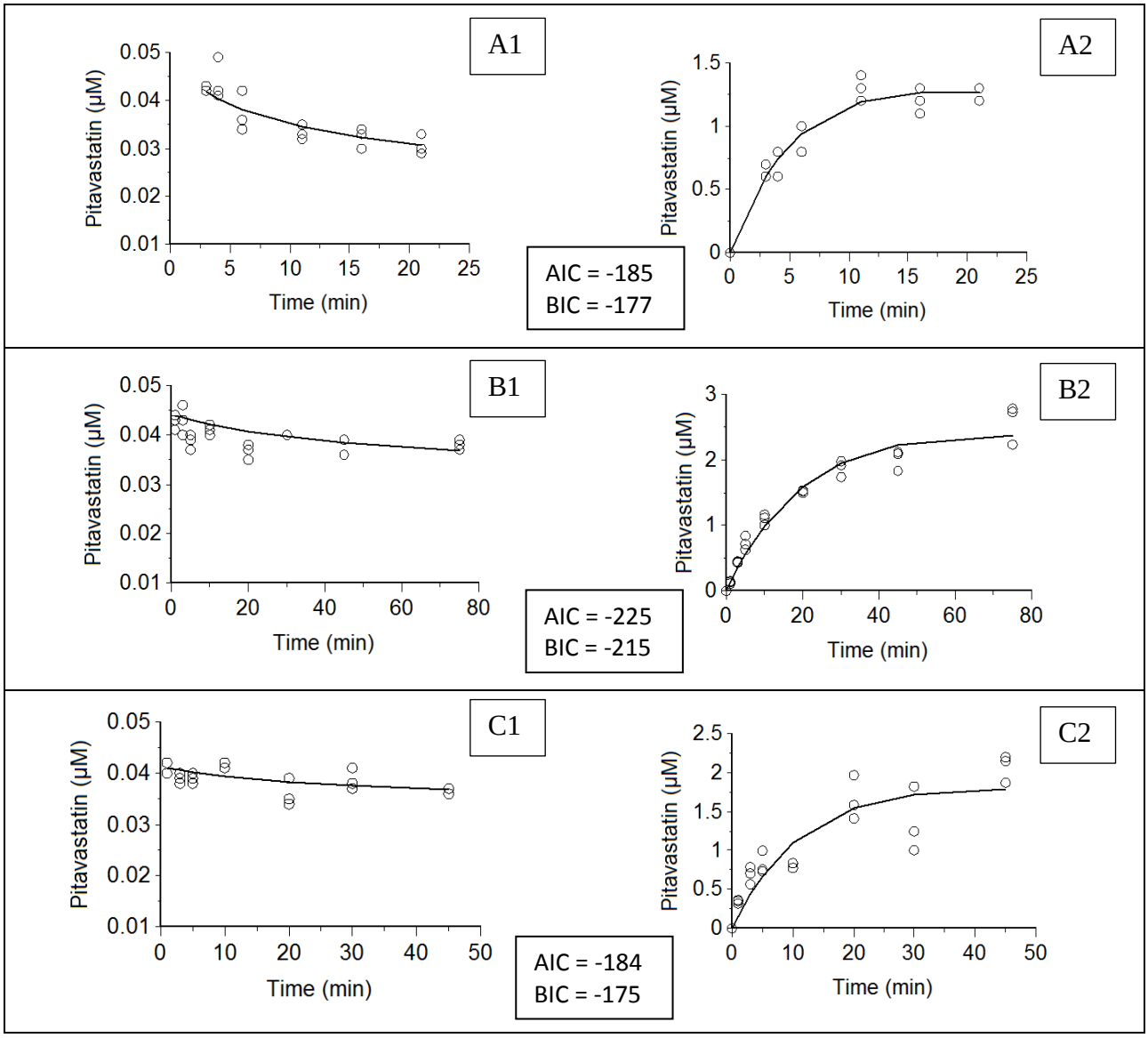

DMD Fast Forward. Published on April 17, 2018 as DOI: 10.1124/dmd.118.080614
This article has not been copyedited and formatted. The final version may differ from this version.

Figure 2

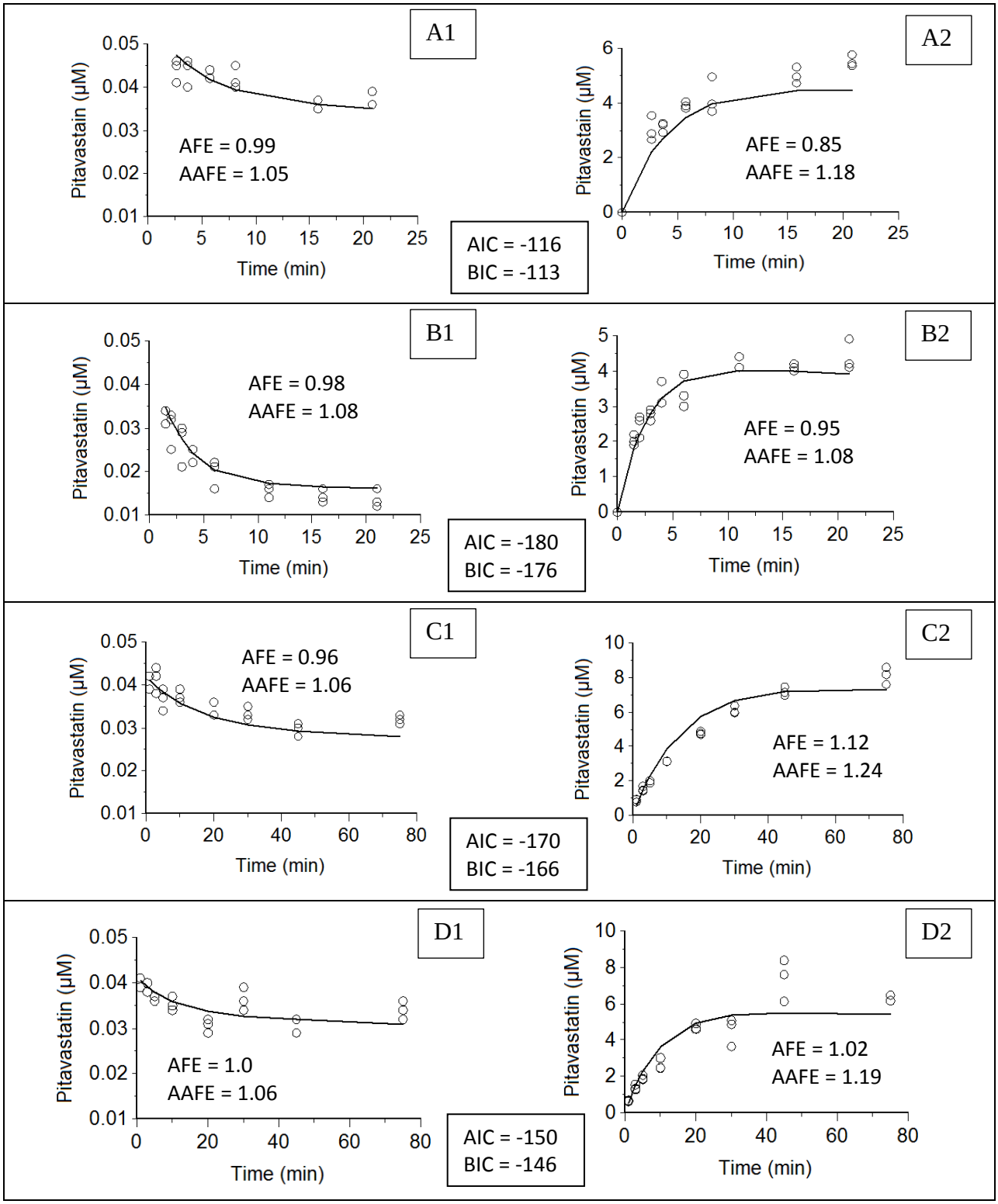

DMD Fast Forward. Published on April 17, 2018 as DOI: 10.1124/dmd.118.080614
This article has not been copyedited and formatted. The final version may differ from this version.

Figure 3

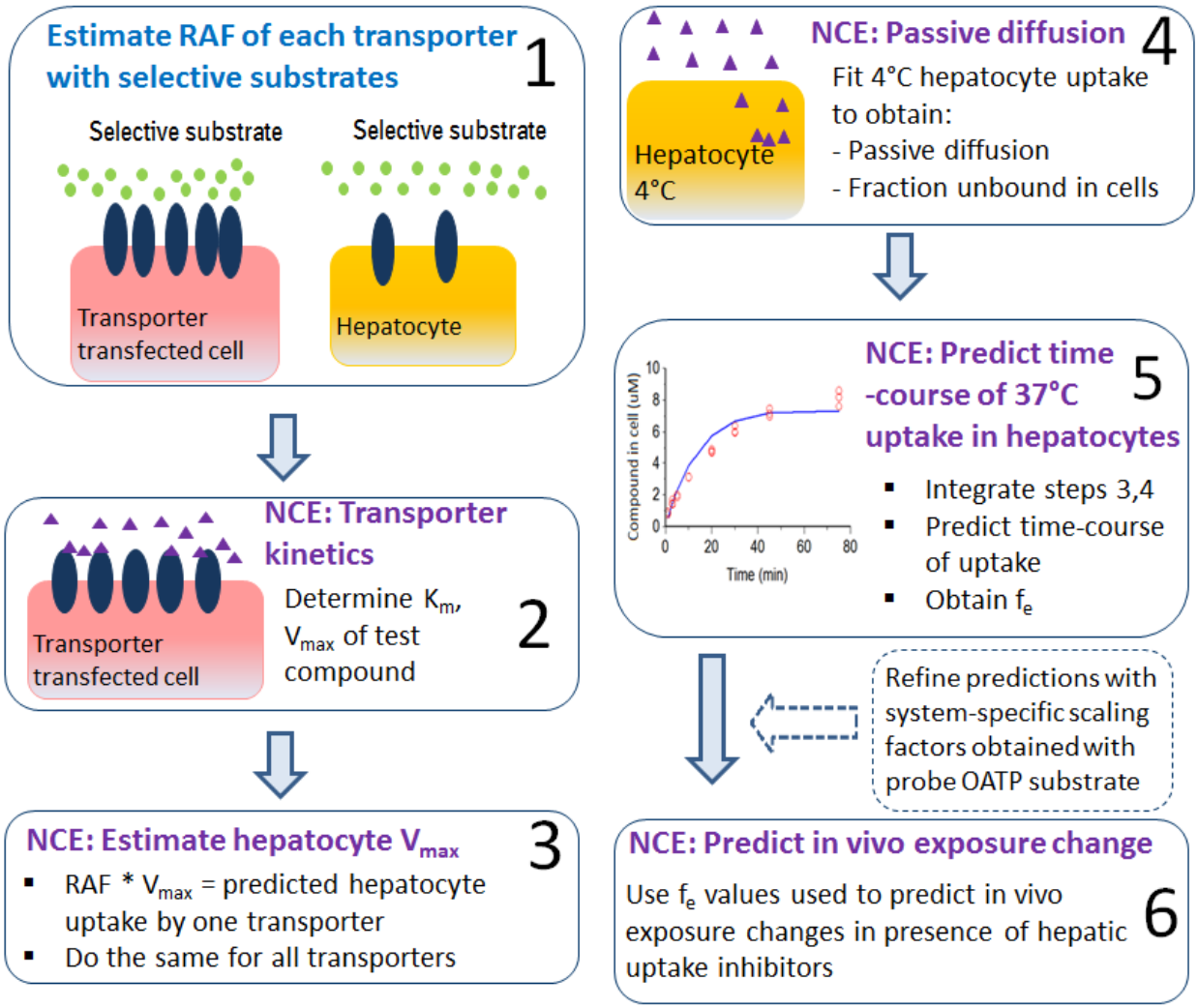

Supplemental data to:

Prediction and quantification of hepatic transporter-mediated uptake of pitavastatin utilizing a combination of the Relative Activity Factor approach and mechanistic modeling

Pallabi Mitra, Samantha Weinheimer, Meeghan Michalewicz, and Mitchell E. Taub

Drug Metabolism and Pharmacokinetics Department, Boehringer Ingelheim Pharmaceuticals, Inc., Ridgefield, CT 06877

Number of pages: 21

Number of supplemental tables: 3

Number of supplemental figures: 5

Supplemental text

Section 1. Phoenix WinNonlin Model codes

Nomenclature of terms used in model codes

A_{med}, is the amount of substrate in medium at time t; A_{cell}, is the amount of substrate in cells at time t; $CL_{passive}$, is passive diffusion mediated clearance (µL/min/mg); TP, is total protein (mg); C_{med}, is the total concentration of compound in the medium at time t (µM); C_{cell}, is the total concentration of compound in the cells at time t (µM); f_{um} is fraction unbound in medium (unitless); f_U is fraction unbound in cells (unitless); nsb, is non-specific binding (min^{-1}); V_{med}, is volume of media; V_{cell}, is volume of cells; $V_{max\_transporter}$ is the predicted V_{max} of pitavastatin for that transporter (pmol/min/mg); $K_{m\_transporter}$ is the K_m of pitavastatin for that transporter (µM).

Phoenix WinNonlin modeling code for fitting hepatocyte disposition of pitavastatin at 4°C

```
test(){
    deriv(Amed = - (CLpassive * TP*(Cmed*fum - (Ccell*fU)))- (Cmed*fum*nsb*Vmed))
    deriv(Acell = (CLpassive * TP*((Cmed*fum) - (Ccell*fU))))
    Cmed = Amed / Vmed
    dosepoint(Amed, idosevar = AmedDose)
    error(CEps = 1)
    observe(CObs = Cmed + CEps)
    Ccell = Acell / Vcell
    error(CcEps = 1)
    observe(CObs_cell = Ccell + CcEps)
    stparm(Vmed = tvVmed)
    stparm(Vcell = tvVcell)
    stparm(CLpassive = tvCLpassive)
    stparm(TP = tvTP)
    stparm(fum = tvfum)
    stparm(fU = tvfU)
```

```
        stparm(nsb = tvnsb)

        fixef(tvVmed (freeze)   = c(, 500, ))

        fixef(tvVcell (freeze) = c(, 0.75, ))

        fixef(tvCLpassive    = c(, 7, ))

        fixef(tvTP(freeze) = c(, 0.090, ))

        fixef(tvfU    = c(, 0.053, ))

        fixef(tvfum (freeze)    = c(, 1, ))

        fixef(tvnsb       = c(0, 0.0013, ))

}
```

Phoenix WinNonlin modeling code for predicting hepatocyte disposition of pitavastatin at 37°C

```
test(){

        deriv(Amed = - (CLpassive * TP*(Cmed*fum - (Ccell*fU)))- (Cmed*nsb*Vmed) -
(((Vmax_OATP1B1*TP)/(Km_OATP1B1 + Cmed*fum)) * Cmed*fum)-
(((Vmax_OATP1B3*TP)/(Km_OATP1B3 + Cmed*fum)) * Cmed*fum)-
(((Vmax_NTCP*TP)/(Km_NTCP + Cmed*fum)) * Cmed*fum)-
(((Vmax_MRP3*TP)/(Km_MRP3 + (Ccell*fU))) * (Ccell*fU)))

        deriv(Acell = (CLpassive * TP*(Cmed*fum - (Ccell*fU))) +
(((Vmax_OATP1B1*TP)/(Km_OATP1B1 + Cmed*fum)) * Cmed*fum) +
```

```
(((Vmax_OATP1B3*TP)/(Km_OATP1B3 + Cmed*fum)) * Cmed*fum) +
(((Vmax_NTCP*TP)/(Km_NTCP + Cmed*fum)) * Cmed*fum) -
(((Vmax_MRP3*TP)/(Km_MRP3 + (Ccell*fU))) * (Ccell*fU)))

        Cmed = Amed / Vmed

        dosepoint(Amed, idosevar = AmedDose)

        error(CEps = 1)

        observe(CObs = Cmed + CEps)

        Ccell = Acell / Vcell

        error(CcEps = 1)

        observe(CObs_cell = Ccell + CcEps)

        stparm(Vmed = tvVmed)

        stparm(Vcell = tvVcell)

        stparm(CLpassive = tvCLpassive)

        stparm(Vmax_OATP1B1 = tvVmax_OATP1B1)

        stparm(Km_OATP1B1 = tvKm_OATP1B1)

        stparm(Vmax_OATP1B3 = tvVmax_OATP1B3)

        stparm(Km_OATP1B3 = tvKm_OATP1B3)

        stparm(Vmax_NTCP = tvVmax_NTCP)
```

```
stparm(Km_NTCP = tvKm_NTCP)

stparm(Vmax_MRP3 = tvVmax_MRP3)

stparm(Km_MRP3 = tvKm_MRP3)

stparm(TP = tvTP)

stparm(fum = tvfum)

stparm(fU = tvfU)

stparm(nsb = tvnsb)

fixef(tvVmed (freeze)  = c(, 500, ))

fixef(tvVcell (freeze)   = c(, 0.75, ))

fixef(tvCLpassive (freeze)    = c(, 23.78, ))

fixef(tvVmax_OATP1B1 (freeze)     = c(, 214.9, ))

fixef(tvKm_OATP1B1 (freeze)     = c(0, 4.22, ))

fixef(tvVmax_OATP1B3 (freeze)   = c(,23.1, ))

fixef(tvKm_OATP1B3 (freeze) = c(, 2.24, ))

fixef(tvVmax_NTCP(freeze) = c(, 244.67, ))

fixef(tvKm_NTCP(freeze) = c(, 24.28, ))

fixef(tvVmax_MRP3 (freeze) = c(, 0.1272, ))
```

```
fixef(tvKm_MRP3(freeze) = c(, 448, ))

fixef(tvTP (freeze) = c(,0.101, ))

fixef(tvfU (freeze)     = c(, 0.0154, ))

fixef(tvfum (freeze)    = c(, 1, ))

fixef(tvnsb (freeze)    = c(, 0.00130, ))
```

}

Section 2 Methodology of estimation of uptake kinetics of transporters in hepatocytes (suspensions and SCHH).

Suspended Hepatocytes. The protocol used here to assess uptake in hepatocyte suspensions was based on the BioreclamationIVT *Cryopreserved Hepatocyte Uptake Transporter Assay*. An orbital shaker was placed in a 37 ^{o}C incubator without humidity and CO_2 in order to evaluate total uptake and wet ice was placed on a separate orbital shaker to evaluate passive uptake at 4 ^{o}C. Passive uptake of E3S by OATP1B1 was also evaluated at 37 ^{o}C by adding 100 uM rifamycin directly to the substrate solution. In 0.4 ml tubes, a 100 µl layer of 2N NaOH was topped with a 100 µl layer of filtration oil consisting of a 5:1 silicone oil to mineral oil mixture. On the day of the assay, all substrate solutions containing the radio-labeled compounds were prepared. Substrate solutions were prepared in KHB for all assays assessing the OATP1B1 and OATP1B3 transporters as well as total uptake by NTCP while the sodium-free buffer made in-house was used when assessing the passive uptake by the NTCP transporter. Solutions were allowed to acclimate to 37 ^{o}C in the incubator or to 4 ^{o}C on wet ice. Wash buffers corresponding to the buffers used to make the solutions were allowed to chill to 4 ^{o}C in wet ice.

After cells acclimated for 15 minutes in the 37 ^{o}C incubator or to 4 ^{o}C on the wet ice, the orbital shakers were set to 250 rpm for the remainder of the experiment. Uptake was initiated by adding 50 µl of substrate solution to the wells containing 100 ul of suspended cells. Incubation times for each transporter were predetermined by conducting time-dependent assays using a single concentration of each radio-labeled substrate. The incubation times determined and used in all kinetic assays were as follows: 1 minute for the uptake of E3S and pitavastatin by OATP1B1, and 3 minutes for the uptake of TCA and CCK-8 by NTCP and OATP1B3 respectively. At the end of the incubation time, the suspension was quickly pipetted from each well and added to its respective 0.4 ml tube containing the filtration oil and 2N NaOH. The tubes were immediately centrifuged at 14,000 rpm for 1 minute to allow the cells to travel through the filtration oil to the 2 N NaOH. Each tube was placed into dry ice for at least 20 minutes. The tubes were then cut in the middle oil layer. The bottom layer of each tube containing the cell pellet was dropped into a corresponding well of a 12-well cell culture plate where 500 µl of a 1% SDS solution in distilled water was added to each well to lyse the cells. The lysates were shaken at 250 rpm for at least one hour on an orbital shaker at room temperature. The solution was then pipetted into a 4 ml scintillation vial. To each vial, 3 ml of Optiphase Supermix Cocktail was added and the samples were analyzed on the Perkin Elmer MicroBeta2. All substrate solutions were analyzed as well to more accurately determine the total concentration of radio-labeled compound added.

Sandwich Cultured Human Hepatocytes (SCHH). Five days after addition of the Matrigel to the plated hepatocytes, the uptake assay was carried out. Substrate solutions were prepared in KHB for all assays assessing the OATP1B1 and OATP1B3 transporters as well as total uptake by NTCP while the sodium-free buffer made in-house was used when assessing the

passive uptake by the NTCP transporter. Solutions were allowed to acclimate to 37 ^{o}C in the incubator without humidity and CO_2 or to 4 ^{o}C on wet ice. Wash buffers corresponding to the buffers used to make the solutions were allowed to chill to 4 ^{o}C in wet ice. Total uptake was assessed at 37 ^{o}C while passive uptake was assessed at 4 ^{o}C on wet ice. Passive uptake of E3S by OATP1B1 was also evaluated at 37 ^{o}C by adding 100 uM rifamycin directly to the substrate solution. To each well, 500 ul of substrate solution containing radio-labeled compound was added and incubated for the appropriate time. Incubation times for each transporter were predetermined by conducting time-dependent assays using a single concentration of each radio-labeled substrate. The incubation times determined and used in all kinetic assays were as follows: 1 minute for the uptake of E3S and pitavastatin by OATP1B1, and 3 minutes for the uptake of TCA and CCK-8 by NTCP and OATP1B3 respectively. At the end of the incubation, the solutions were either aspirated into a waste container or pipetted into a 1.5 ml Eppendorf tube. The cells were then washed 3x with ice cold wash buffer. To lyse the cells, 500 µl of a 1% SDS solution in distilled water was added to each well. The plates were allowed to shake on an orbital shaker at 250 rpm for at least 1 hour at room temperature. The samples were then transferred to 4 ml scintillation vials. To each vial, 3 ml of Optiphase Supermix Cocktail was added. Each sample was analyzed on the Perkin Elmer MicroBeta2. All substrate solutions were analyzed as well to more accurately determine the total concentration of radio-labeled compound added. The solutions that were removed from the cells and placed in 1.5 ml tubes were analyzed in order to determine the mass balance of the compound.

Supplemental Tables

Table S1: Donor characteristics of hepatocyte lots

Hepatocyte lot	Gender, Age, Race	Transporter certification			
		Vendor certification	Internal qualification: Active uptake of 0.1 µM E3S (µL/min/mg) in:		
			Suspension	2 h after plating	144 h after plating
HUM4122D (Single donor)	F,35, Asian	Rosuvastatin uptake = 179% of historical database	235 ± 33	73 ±12	102 ± 27
Hu1651 (Single donor)	F, 60, Caucasian	Active uptake of 1 µM estradiol 17β glucuronide = 4.9 pmol/min/mg	ND	78 ± 19	54 ± 7
HUP1001 (Pooled)	Mixed, NA, NA	None	58 ± 18	NA[a]	NA[a]

NA: Not applicable

ND: Not done due to limited availability of this hepatocyte lot.

NA[a]: Pooled hepatocytes, not amenable to plating.

Table S2: Sensitivity analysis of the impact of MRP3 on intracellular accumulation of pitavastatin.

Cellular accumulation of pitavastatin was simulated for several hypothetical situations where MRP3 V_{max} was considered to be either 0 or some arbitrary fold of the original V_{max}. The % change in cellular AUC was calculated with respect to the AUC obtained under 'V_{max} = original' condition.

MRP3 V_{max}	**Pitavastatin cellular AUC (nM.h)**	**% change in cellular AUC**
V_{max} = original	456.9436	NA
V_{max} = 0	456.9467	0.0007
V_{max} = 1X original	456.9162	-0.0060
V_{max} = 10X original	456.6418	-0.0661
V_{max} = 100X original	453.9143	-0.6630
V_{max} = 10^4X original	428.2350	-6.2828
V_{max} = 10^5X original	271.2154	-40.6458

NA: Not applicable

Table S3: Physicochemical properties and pharmacokinetic parameters of rifampicin and cyclosporine reported in the literature that were utilized for predicting AUCR values resulting from hepatic uptake inhibition of pitavastatin

Perpetrator drug	Pharmacokinetic parameters									
	Dose (mg)	C_{max} (µg/mL)	K_a min^{-1}	F_a	F_g	f_u	R_b	K_i (µM)		
								OATP 1B1	OATP 1B3	NTCP
Rifampicin	600	10[a]	0.021[b]	1[c]	0.99[c]	0.13[d]	0.9[c]	0.09[e]	0.03[e]	138.5[a]
Cyclosporine	175[f,g]	0.92[f, g]	0.039[h,i]	0.86[c]	0.48[c]	0.068[j]	1.93[k]	0.014[l]	0.007[l]	0.28[l]

C_{max}: Maximum plasma concentration associated with that drug dose; AUCR=Ratio of AUCs with and without the inhibitor; K_a: Absorption rate constant; F_a: Fraction available after absorption; F_g: Fraction available after escaping metabolism in the gut; f_u: fraction unbound in plasma; R_b: blood plasma partition co-efficient; K_i: reversible inhibition constant; SD: single dose

[a] Prueksaritanont, T., et al., (2014)

[b] Peloquin, C.A., et al., (1997)

[c] Varma, M.V., et al., (2014)

[d] Boman, G. and V.A. Ringberger (1997)

[e] Duan, P., P. Zhao, and L. Zhang (2016)

[f] Pitavastatin DDI with cyclosporine was observed with 2 mg/kg cyclosporine (NDA application of cyclosporine). The associated plasma exposure of cyclosporine is not available. The C_{max} value in the above table is from a 175 mg oral dose.

[g] Kovarik, J.M., et al., (2002)

[h] Geometric mean of K_a from formulations of Sandimmune® and Neoral®

[i] Monchaud, C. and P. Marquet (2009)

[j] Legg, B., et al., (1988)

[k] Zaghloul, I., et al., (1987)

[l] Jamei, M., et al., (2014)

References for Supplemental Tables

Prueksaritanont, T., et al., *Pitavastatin is a more sensitive and selective organic anion-transporting polypeptide 1B clinical probe than rosuvastatin.* Br J Clin Pharmacol, 2014. **78**(3): p. 587-98.

Peloquin, C.A., et al., *Population pharmacokinetic modeling of isoniazid, rifampin, and pyrazinamide.* Antimicrob Agents Chemother, 1997. **41**(12): p. 2670-9.

Varma, M.V., et al., *Quantitative prediction of transporter- and enzyme-mediated clinical drug-drug interactions of organic anion-transporting polypeptide 1B1 substrates using a mechanistic net-effect model.* J Pharmacol Exp Ther, 2014. **351**(1): p. 214-23.

Boman, G. and V.A. Ringberger, *Binding of rifampicin by human plasma proteins.* Eur J Clin Pharmacol, 1974. **7**(5): p. 369-73.

Duan, P., P. Zhao, and L. Zhang, *Physiologically Based Pharmacokinetic (PBPK) Modeling of Pitavastatin and Atorvastatin to Predict Drug-Drug Interactions (DDIs).* Eur J Drug Metab Pharmacokinet, 2016.

Kovarik, J.M., et al., *Differential influence of two cyclosporine formulations on everolimus pharmacokinetics: a clinically relevant pharmacokinetic interaction.* J Clin Pharmacol, 2002. **42**(1): p. 95-9.

Monchaud, C. and P. Marquet, *Pharmacokinetic optimization of immunosuppressive therapy in thoracic transplantation: part I.* Clin Pharmacokinet, 2009. **48**(7): p. 419-62.

Legg, B., et al., *Cyclosporin: pharmacokinetics and detailed studies of plasma and erythrocyte binding during intravenous and oral administration.* Eur J Clin Pharmacol, 1988. **34**(5): p. 451-60.

Zaghloul, I., et al., *Blood protein binding of cyclosporine in transplant patients.* J Clin Pharmacol, 1987. **27**(3): p. 240-2.

Jamei, M., et al., *A mechanistic framework for in vitro-in vivo extrapolation of liver membrane transporters: prediction of drug-drug interaction between rosuvastatin and cyclosporine.* Clin Pharmacokinet, 2014. **53**(1): p. 73-87.

Supplemental Figure legends

Fig. S1: Uptake of estrone-3-sulfate (A), CCK-8 (B), and taurocholic acid (C) in HEK293 cells transfected with OATP1B1, OATP1B3, and NTCP, respectively. Uptake of pitavastatin in HEK293-OATP1B1 (D), HEK293-OATP1B3 (E), and HEK293-NTCP (F) cells, respectively. Experimental data are presented as mean ± SD (n = 3). Each experiment was repeated at least twice, except C which was done once.

Fig. S2: Uptake of estrone-3-sulfate, CCK-8, and taurocholic acid in suspension hepatocytes (A-D lot HUP1001, E-H lot HUM4122D. Experimental data are presented as mean ± SD (n = 3). RIF = Rifamycin SV.

Fig. S3: Uptake of estrone-3-sulfate, CCK-8, and taurocholic acid in SCHH (A-C lot HU1651, D-G lot HUM4122D). Experimental data are presented as mean ± SD (n = 3). RIF = Rifamycin SV. Of note, E3S uptake kinetics with rifamycin SV were not done in lot Hu1651 since this lot had limited supply, and other experiments were prioritized in this lot of hepatocytes.

Fig. S4: Individual predicted concentrations versus observed concentrations for pitavastatin in media (A1- C1) and in cells (A2 -C2) at 4°C. The solid line is the line of unity, and open circles represent observed data (individual values). A1, A2: suspension, lot HUM4122D; B1, B2: SCHH lot HUM4122D; C1, C2: SCHH lot Hu1651.

Fig. S5: Individual predicted concentrations versus observed concentrations for pitavastatin in media (A1-D1) and in cells (A2-D2) at 37°C. The solid line is the line of unity, and open circles represent observed data (individual values). A1, A2: suspension, lot HUP1001; B1, B2: suspension, lot HUM4122D; C1, C2: SCHH lot HUM4122D; D1, D2: SCHH lot Hu1651.

Supplemental Figures

Figure S1

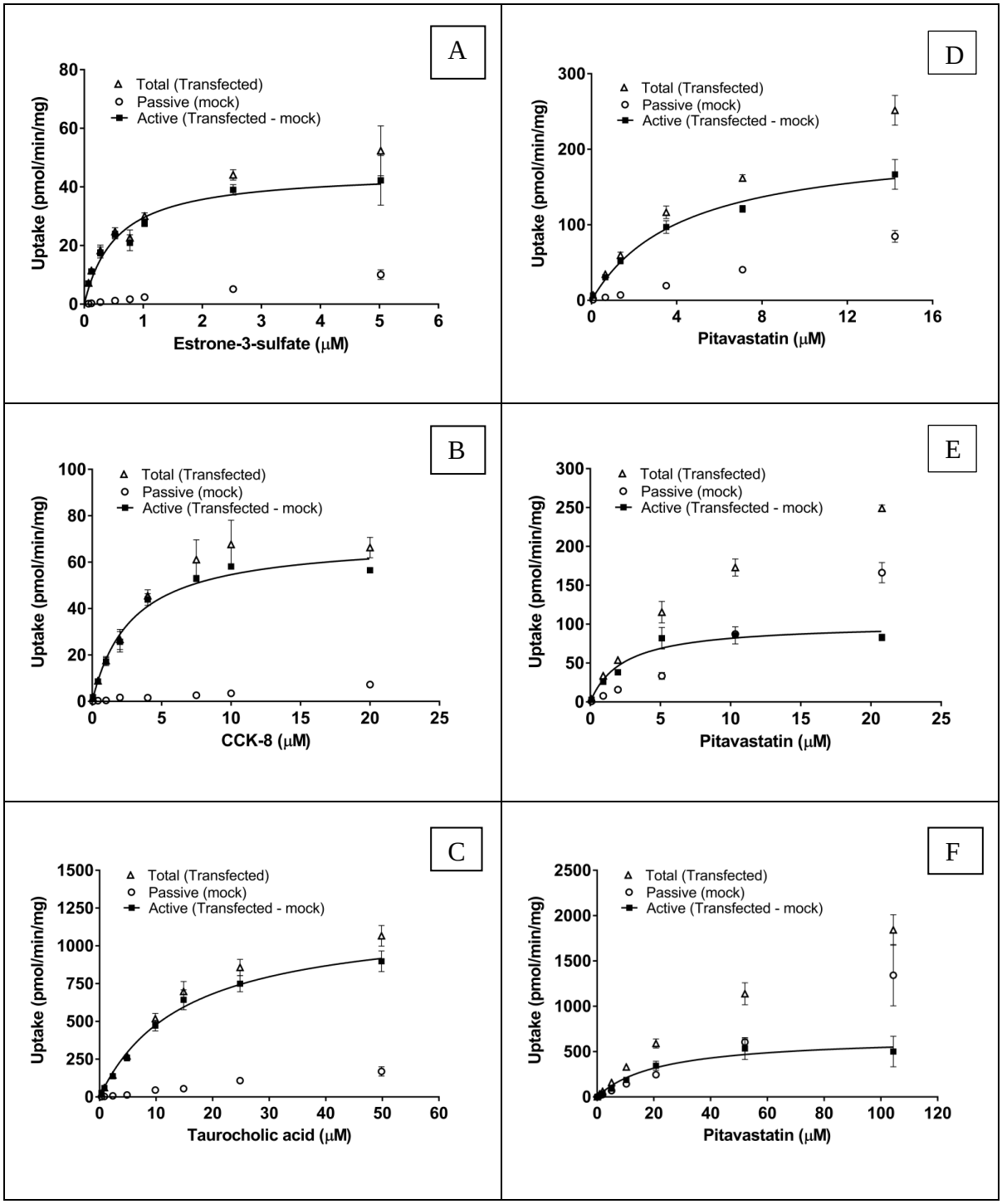

Figure S2

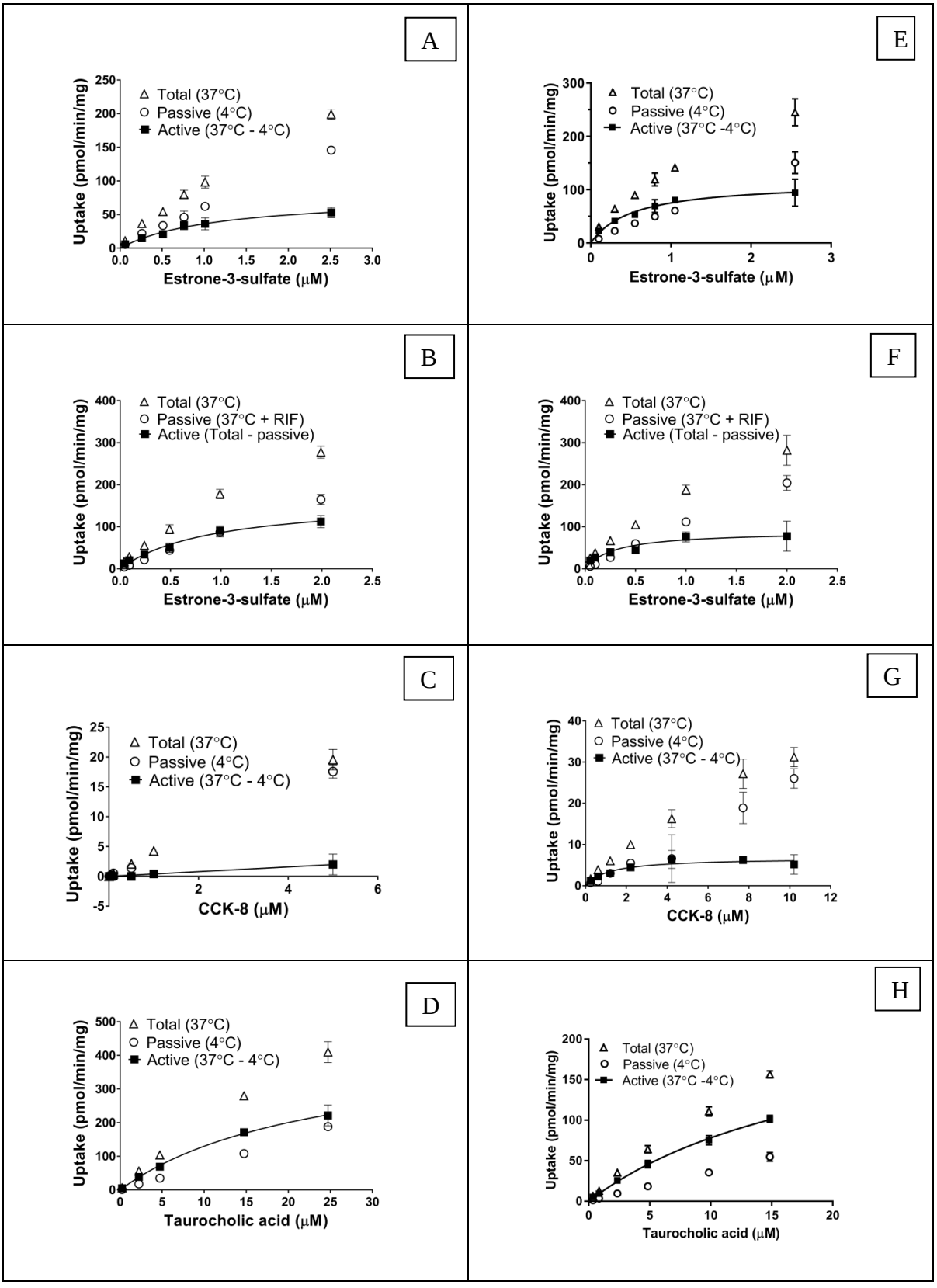
A
Total (37°C)
Passive (4°C)
Active (37°C - 4°C)
Uptake (pmol/min/mg)
Estrone-3-sulfate (μM)
E
Total (37°C)
Passive (4°C)
Active (37°C -4°C)
Uptake (pmol/min/mg)
Estrone-3-sulfate (μM)
B
Total (37°C)
Passive (37°C + RIF)
Active (Total - passive)
Uptake (pmol/min/mg)
Estrone-3-sulfate (μM)
F
Total (37°C)
Passive (37°C + RIF)
Active (Total - passive)
Uptake (pmol/min/mg)
Estrone-3-sulfate (μM)
C
Total (37°C)
Passive (4°C)
Active (37°C - 4°C)
Uptake (pmol/min/mg)
CCK-8 (μM)
G
Total (37°C)
Passive (4°C)
Active (37°C - 4°C)
Uptake (pmol/min/mg)
CCK-8 (μM)
D
Total (37°C)
Passive (4°C)
Active (37°C - 4°C)
Uptake (pmol/min/mg)
Taurocholic acid (μM)
H
Total (37°C)
Passive (4°C)
Active (37°C -4°C)
Uptake (pmol/min/mg)
Taurocholic acid (μM)

Figure S3

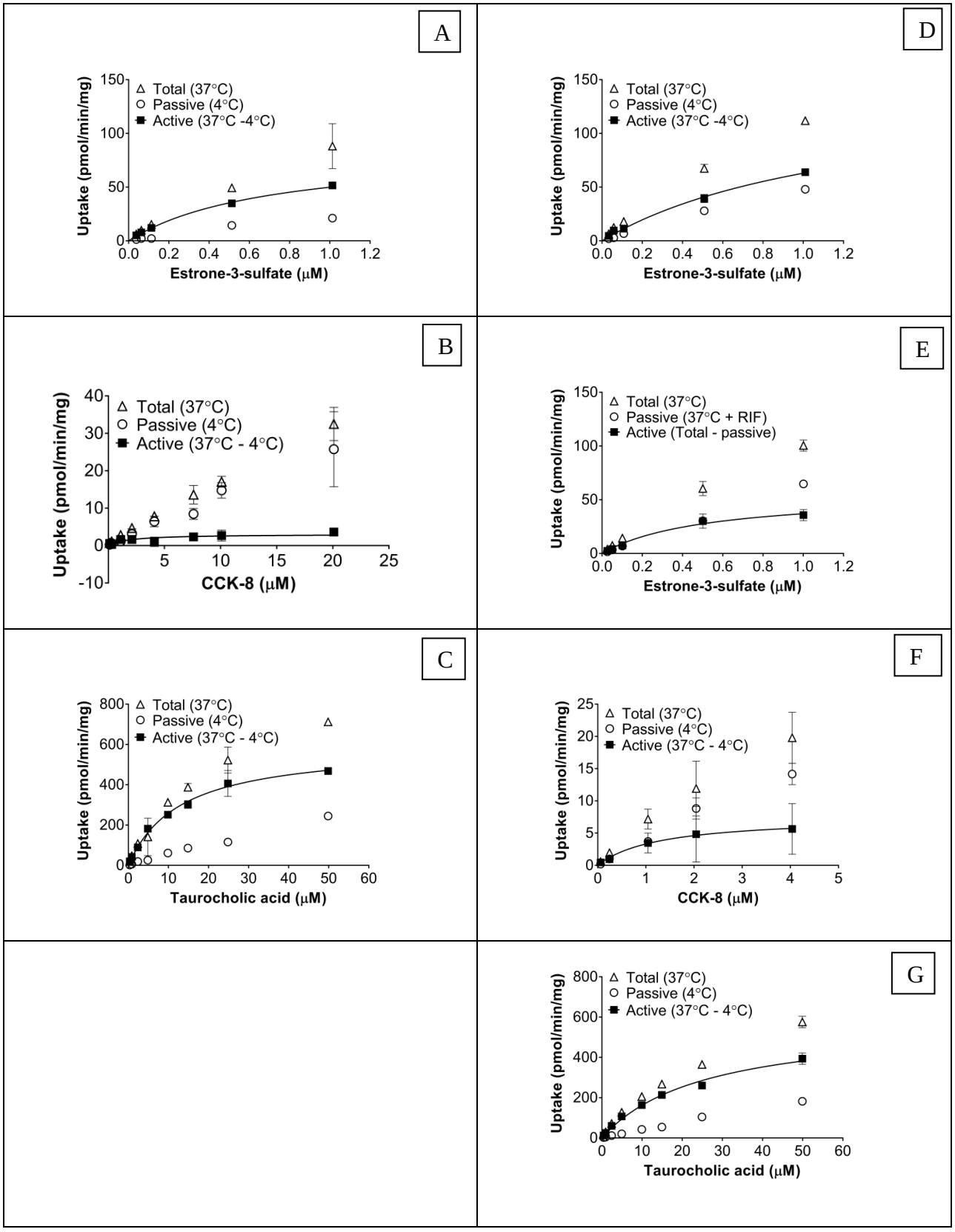
A
Total (37°C)
Passive (4°C)
Active (37°C -4°C)
Uptake (pmol/min/mg)
Estrone-3-sulfate (μM)
D
Total (37°C)
Passive (4°C)
Active (37°C -4°C)
Uptake (pmol/min/mg)
Estrone-3-sulfate (μM)
B
Total (37°C)
Passive (4°C)
Active (37°C - 4°C)
Uptake (pmol/min/mg)
CCK-8 (μM)
E
Total (37°C)
Passive (37°C + RIF)
Active (Total - passive)
Uptake (pmol/min/mg)
Estrone-3-sulfate (μM)
C
Total (37°C)
Passive (4°C)
Active (37°C - 4°C)
Uptake (pmol/min/mg)
Taurocholic acid (μM)
F
Total (37°C)
Passive (4°C)
Active (37°C - 4°C)
Uptake (pmol/min/mg)
CCK-8 (μM)
G
Total (37°C)
Passive (4°C)
Active (37°C - 4°C)
Uptake (pmol/min/mg)
Taurocholic acid (μM)

Figure S4

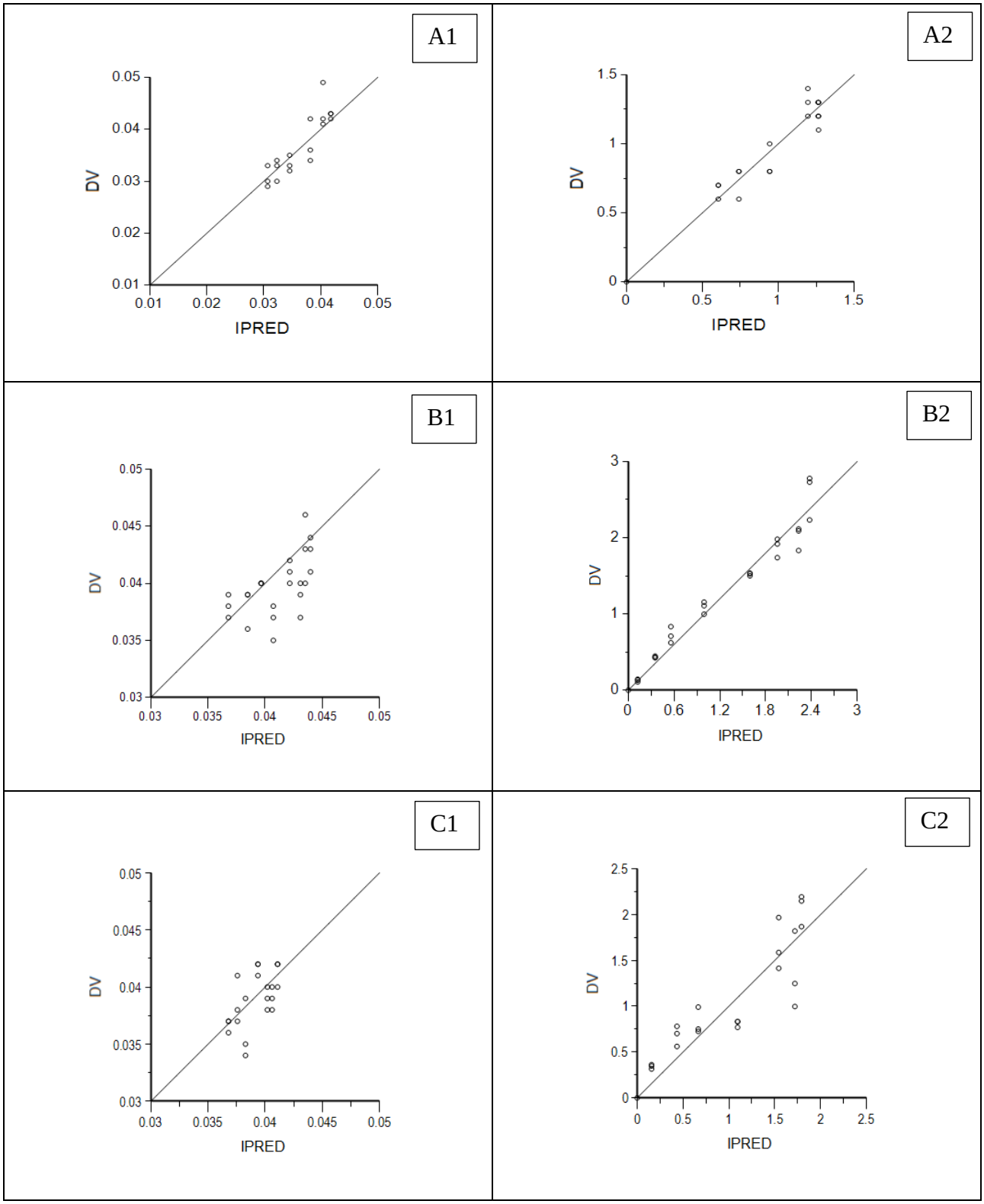
A1
DV
IPRED
0.05
0.04
0.03
0.02
0.01
A2
1.5
1
0.5
0
B1
0.045
0.035
B2
3
2
0.6
1.2
1.8
2.4
C1
C2
2.5

Figure S5